Powder Technology 466 (2025) 121504

Contents lists available at ScienceDirect

Powder Technology

journal homepage: www.journals.elsevier.com/powder-technology

Experimental investigation of the effect of magnetic field placement on pressure drop, entropy generation, heat transfer, and thermal performance of Fe_3O_4/TiO_2 magnetic nanofluids in turbulent flow

Victor O. Adogbeji [a,e], Kuvendran Govinder [a], Mohsen Sharifpur [a,b,c,*], Josua P. Meyer [a,d]

[a] Department of Mechanical and Aeronautical Engineering, University of Pretoria, Pretoria, Private Bag X20, Hatfield 0028, South Africa
[b] School of Mechanical, Industrial and Aeronautical Engineering, University of the Witwatersrand, Private Bag 3, Wits 2050, South Africa
[c] Department of Medical Research, China Medical University, Taichung, Taiwan
[d] Department of Mechanical and Mechatronic Engineering, Stellenbosch University, Stellenbosch, South Africa
[e] Department of Mechanical and Industrial Engineering Technology, University of Johannesburg, Johannesburg, Private Bag,2092, South Africa

HIGHLIGHTS:

- Magnetic field improves heat transfer, reduces entropy in Fe_3O_4/TiO_2 nanofluids.
- High nanoparticle loading raises pressure drop, lowers thermal efficiency.
- Square Wave Case II yields 28.21 % CHT rise at 0.0125 % nanoparticle volume.
- Lower nanoparticle loads give better CHT gains; higher loads reduce it.
- Magnetic field position alters thermal performance; Case IV shows less gain.

GRAPHICAL ABSTRACT

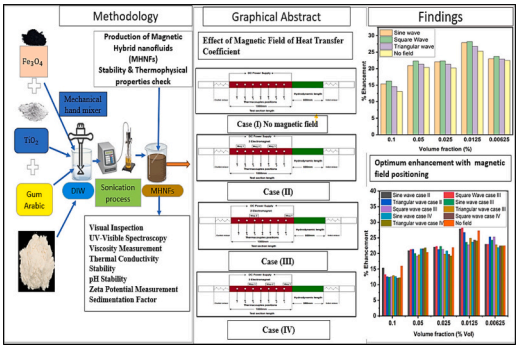

ARTICLE INFO

Keywords:
Magnetic waveform placement
MHNFs hybrid nanofluid
Pressure drop
Entropy generation
Thermal performance factor
Turbulent forced convection

ABSTRACT

Utilizing magnetic fields to manipulate fluid motion in ferrofluids has become a crucial approach for improving heat exchange efficiency in thermal applications, especially in pipe systems. This research conducts an experimental analysis of the effects of magnetic field (MF) patterns on heat transfer, entropy production, and the thermal efficiency of Fe_3O_4/TiO_2 magnetic hybrid nanofluids (MHNFs) operating under turbulent flow regimes. Key parameters explored include nanoparticle concentration, effect of magnetic field placement, and signal waveform types (square, sine, and triangular). Results demonstrate that lower nanoparticle concentrations (0.0125–0.1 vol%) significantly improve thermal performance compared to deionized water and higher concentrations. The square waveform yielded the highest heat transfer enhancement (28.21 %), followed by sine (27.87 %) and triangular waveforms (22.81 %). Additionally, entropy generation was minimized through optimized magnetic field application and placement, highlighting its critical role in improving heat transfer efficiency.

The thermal performance (TP) peaked at 26.33 % enhancement with 0.0125 vol%, while lower pressure drops were observed at 0.0125 vol% to be 7.67 %, and 0.00625 vol%, corresponding to 10.29 %. This study introduces

* Corresponding author at: Department of Mechanical and Aeronautical Engineering, University of Pretoria, Pretoria, Private Bag X20, Hatfield 0028, South Africa.
E-mail address: mohsen.sharifpur@up.ac.za (M. Sharifpur).

https://doi.org/10.1016/j.powtec.2025.121504
Received 18 January 2025; Received in revised form 27 July 2025; Accepted 30 July 2025
Available online 31 July 2025

a novel approach to optimizing heat transfer systems by integrating magnetic field waveform placement with precise nanoparticle formulations. The findings have significant implications for advancing energy-efficient cooling systems in thermal management applications, offering enhanced heat transfer with reduced energy losses.

Abbreviations

Al	Aluminium nanoparticles
AL_2O_3	Aluminium oxide nanoparticles
Au	Gold nanoparticles
C_p	Specific heat transfer
Co_2O_3	Cobalt (III) oxide nanoparticles
Cu	Copper nanoparticles
CuO	Copper oxide nanoparticles
CHT	Convective heat transfer
CNTs	Carbon nanotubes
DC	Direct current
Di	Internal diameter of the tube
DIW	Deionized water
DW	Distilled water
EC	Electrical conductivity
EG	Ethylene glycol
Fe_2O_3	Iron (III) oxide nanoparticles
Fe_3O_4	Iron (IV) oxide nanoparticles
G	Gauss
GA	Gum Arabic
GMO	Graphene magnetite oxide
I	Current (Ampere)
$\dot{m}$	Mass flow rate
MF	Magnetic fields
MFS	Magnetic fields strength
MHNFs	Magnetic hybrid nanofluids
MNFs	Magnetic nanofluids
MNPs	Magnetic nanoparticles
MWCNT	Multiwalled carbon nanoparticle
$\dot{q}$	Heat flux, W/m^2
SF	Sedimentation Factor
SiO_2	Silicon oxide nanoparticles
TC	Thermal conductivity
TEM	Transmission electron microscopy
TiO_2	Titanium oxide nanoparticles
TEI	Total efficiency index
UV–Vis	Ultra Violet-Visible
V	Voltage
x/d	Axial distance

Greek symbols

φ	Mass ratio of nanofluids
Φ	Volume concentration (vol%)
μ	Viscosity (kg/m.s)
κ	Thermal conductivity (W/K-1)
σ	Electrical conductivity (mS/cm −1)
ρ	Density (Kg/m^3)
η	Thermal efficiency
$\dot{q}$	Heat flux, (W/m^2)
$\dot{m}$	Mass flow rate (Kg/s)

Subscripts

A_o	Initial Absorbance
A_t	Final Absorbance
avg	Average
u_B	Bias error
u_p	Precision error
bf	base fluid
C_p	Specific heat capacity of particles (J/kg-K)
C_{pnf}	specific heat capacity of nanofluids (J/kg-K)
C_{pbf}	specific heat capacity of base fluids (J/kg-K)
C_{pnp}	specific heat capacity of nanoparticles (J/kg-K)
ρ_{nf}	Densities of the nanofluid (Kg/m^3)
ρ_{bf}	Density of base fluid (Kg/m^3)
$\varphi\rho_{np}$	Density of nanoparticles (Kg/m^3)
h_{avg}	Average heat transfer coefficient (W/m^2—K)
T_O	outlet °C
T_i	inlet °C
t_w	wall temperature °C
t_b	bulk temperature °C
n_f	nanofluid
n_p	nanoparticles

Dimensionless numbers

Nu	Nusselt number
Re	Reynold number
Pr	Prandtl number

1. Introduction

In pursuing advancing thermal management and heat transfer technologies, integrating innovative approaches has become imperative. One promising avenue involves the synergistic interaction between magnetic fields, fluid dynamics, and heat transfer processes. This study explores the intricate dynamics of hydrodynamics effects induced by a MF in the context of forced convective heat transfer (FCHT), employing MHNFs.

In a pioneering idea introduced by Choi [1], enhanced heat transfer capabilities have recently witnessed significant strides with the introduction of nanofluids (n_f), that seamlessly blends nanoparticles into conventional fluids. Nanofluids, characterized by their exceptional thermal characteristics, have become innovative solutions for enhancing heat exchange in a wide range of applications. Typical applications include the demanding realm of electronics cooling, extending to the evolving fields of energy production. Recently, nanofluids have demonstrated remarkable efficiency as cooling agents in sectors like nuclear power plants, medical technologies, and solar energy systems. [2], thermal management in electronic systems [3], automotive [4], HVAC systems [2], heat exchangers [5], power optimization and materials fabrication [6].

The benefits of nanofluids extend beyond their enhanced thermophysical properties, also encompassing their magnetic properties. The influence of MF on nanofluids in channels like pipes introduces a fascinating dimension to their behavior, leading to the development of the field of magnetohydrodynamics (MHD) [7]. The MHD of nanofluids in pipes explores how magnetic forces affect the behavior of these fluids within restricted channels. [8,9]. This field is of great importance due to its capacity to improve heat transfer across various industries. The core of MHD research focuses on analysing the intricate relationships

Table 1
summarizes key findings from previous studies on the CHT pressure drop characteristics under various magnetic field conditions.

Study	Nanofluid Type	Experimental Conditions	Key Findings
Sha et al. [13]	Fe_3O_4/water	Gradient, uniform, and perpendicular magnetic fields, varying nanofluid concentrations and temperatures	Thermal transfer rates enhanced with greater nanofluid concentration, elevated temperature, and stronger magnetic field strength. Gradient magnetic fields resulted in greater enhancement compared to uniform magnetic fields. Fe_3O_4/water nanofluids showed higher CHT coefficients than distilled water, especially at elevated concentrations and temperatures. Specific magnetic field parameters significantly improved CHT.
Yarahmadi et al. [14],	Fe_3O_4/water	Horizontal copper tubes, constant heat flux, oscillating & constant magnetic fields	Oscillating magnetic fields enhanced heat transfer by 19.8 %. Constant magnetic fields reduced heat transfer, with variations observed based on field configurations and vibrational modes.
Abadeh et al. [15]	Fe_3O_4/water	Straight tubes, laminar flow, constant & alternating magnetic fields	Nusselt number increased by 11.85 % (10 Hz) and 14.8 % (100 Hz). No benefits were observed beyond 100 Hz.
Sun et al. [16]	Fe_3O_4/water	Gradient and magnetic flux density variation	Heat transfer improved by 4.36 % and 32.0 % due to chain-like structures. Pressure drop increased with flow disturbances.
Goharkhah et al. [17]	Fe_3O_4/water	Heated tube, steady & alternating magnetic fields, 1–2 % concentration, *Re* 400–1200	Heat transfer improved up to 31.4 % (alternating field) and 9 % (constant field) at 2 % concentration and $Re = 1200$.
Xuan et al. [18]	Fe_3O_4/water	Microchannels, different magnetic field orientations	Improved heat transfer with parallel magnetic field orientations; varied effects with perpendicular orientations.
Motozawa et al. [19]	Fe_3O_4/water	Rectangular channels, varying magnetic field intensity	Significant heat transfer improvements correlated with increased magnetic field intensity.
Şeşen et al. [20]	Ferromagnetic nanoparticles	Magnetic stirrers generating fields	Enhanced heat exchange due to particle circulation in magnetic fields.
Li and Xuan [21]	Fe_3O_4	Around heated wires, magnetic field gradients parallel to flow	Increased heat transfer due to particle migration and interactions.
Mei et al. [22]	Fe_3O_4/water	Copper tubes, varying nanoparticle concentrations, Reynolds numbers, parallel magnetic induction	*Nu* improved with nanoparticle weight percentages, but reduced as magnetic field strength increased.
Azizian et al. [23]	Magnetite nanofluids	Laminar flow, external magnetic fields	Heat transfer coefficients improved significantly with higher magnetic field strength and gradients.
Wang et al. [24]	Fe_3O_4	Tubes, permanent magnetic fields	Substantial heat transfer improvements with increasing magnetic flux density and multiple magnetic cannula configurations.
Mehrali et al. [25]	Graphene-Fe_3O_4nanofluids	Permanent magnetic field	Heat transfer improved significantly with 41 % reduction in entropy generation rate compared to DI water.
Lee et al. [10]	Cobalt zinc ferrite nanofluid	Ethylene glycol/water base, *Re* 1000–1600, magnetic field up to 750 G	Heat transfer improved by 23.9 % at 0.2 wt%. Magnetic field increased efficiency by 2.64 % but led to a 17 % increase in pressure drop at higher strengths.
Shahsavar et al. [26]	Nanofluids	Varying magnetic field strengths	Heat transfer improved by 2.78 %–3.23 % under magnetic fields for specific nanofluid compositions.
Tekir et al. [27]	Fe_3O_4-Cu/water hybrid nanofluid	Constant magnetic field	Nusselt number increased by 14 % under constant magnetic fields, with higher flow rates further improving heat transfer.
Shi et al. [28]	MCNT nanofluids	Magnetically controlled fields	Improved heat transfer compared to DI water and Fe_3O_4 nanofluids, especially at lower Reynolds numbers.
Talebi et al. [29]	Cu and Fe_3O_4/Cu	Single and hybrid nanofluids	Heat transfer improved by up to 11.9 % with hybrid nanofluids compared to Cu/water nanofluids.
Alsarraf et al. [30]	Fe_3O_4-CNT nanofluids	Non-uniform magnetic fields	Heat transfer improved by 109.31 % and pressure drop by 25.02 % under magnetic field effects.
Zhang and Zhang [31]	MNFs	Alternating magnetic fields (0–100 Hz, 0.01–0.09 T), nanoparticle volume fractions	Heat transfer improved with higher nanoparticle fractions but beyond 3 %, higher field frequencies had limited impact. Pressure drops increased with higher volume fractions and frequencies.

between nanofluids, channels, and magnetic forces. [10,11]., unveiling their collective impact on fluid movement, thermal performance, and additional characteristics. [12].

The following Table 1 summarizes key findings from previous studies on the FCHT and pressure drop (Δp) characteristics of Fe_3O_4-based fluids with various magnetic field configurations, nanoparticle compositions, and flow regimes. It highlights the experimental parameters, methodologies, and observed enhancements in heat exchange and Δp, providing a comparative overview of the existing literature.

Despite significant advancements in nanofluid research, critical gaps persist in understanding the role of magnetic fields in CHT, particularly under turbulent flow conditions. While magnetic hybrid nanofluids (MHNFs) demonstrate promise for improving thermal exchange, the impact of magnetic field positioning within the thermally developed region remains insufficiently explored. This aspect is vital, as magnetic field placement can profoundly influence flow dynamics, heat transfer rates, and system efficiency.

Existing studies predominantly focus on particle composition and concentration, with limited attention to the synergistic effects of magnetic field application in real-world turbulent scenarios. Moreover, the effect of different magnetic waveform positions on the heat efficiency of MHNFs is poorly understood, leaving a critical gap in designing effective heat transfer systems.

This research addresses these gaps by investigating the effect of magnetic waveform placement on the CHT characteristics of Fe_3O_4/TiO_2 nanofluids in turbulent flow regimes. Focusing on the thermally developed region, it aims to identify optimal magnetic field configurations to enhance heat transfer effectiveness. The findings will provide practical solutions for improving energy efficiency and thermal management in applications such as energy systems, electronics cooling, and industrial processes, paving the way for next-generation heat exchange fluids.

2. Experimental procedure and protocols

2.1. Preparation and analysis of magnetic hybrid nanofluids

For the study, the nanoparticles (n_p) consisting of Fe_3O_4 with purity of 95.5 %, particle sizes ranging from 20 to 30 nm were used. Furthermore, TiO_2 nanoparticles with purity of 99.5 %, and diameter of 18 nm were included with Gum Arabic (GA) with ≥98.5 % purity as dispersing agent, meeting the particle size specifications as per the manufacturer's

Table 2
Thermophysical attributes of the materials examined at ambient temperature.

Characteristics	Deionized water (DIW)	Fe_3O_4	TiO_2
Specific Heat capacity (J/kg.K)	4179	670	692
Thermal conductivity (W/m.K)	0.613	80.4	8.4
shape	–	Plate-like nanosheet	spherical
Density (kg/m^3)	997	4950	4175

Source: Material Data sheets from Nano Research Materials Inc. Houston, Texas (USA)(US4314)

guidelines. These materials were sourced from Nanostructured and Amorphous Materials Inc. USA and Sigma-Aldrich, Germany, and utilized as a dispersing agent. Table 2 presents the thermal characteristics material properties used.

The synthesis of MHNFs follows a structured five-stage process.

Stage 1: The nanoparticles (n_p), consisting of Fe_3O_4 and TiO_2 in an 80:20 proportion, are carefully measured.

Stage 2: Gum Arabic is added as a stabilizing agent at a weighting factor of 0.75 to enhance the stability of the n_p.

Stage 3: The n_p are initially dispersed in DIW and mixed mechanically, followed by ultrasonic treatment using a controlled pulsing cycle.

Stage 4: The dispersion process is conducted under a controlled environment at 20 °C to ensure consistency.

Stage 5: The MHNFs are then prepared at volume fractions ranging from 0.00625 % to 0.1 % and analyzed for their stability and thermophysical properties.

Fig. 1 illustrates this preparation process, and Eq. (1) [32,33] is employed to calculate the nanoparticle concentrations.

$$\varphi = \left(\frac{Y_{Fe_3O_4}\left(\frac{W}{\rho}\right)_{Fe_3O_4} + Y_{TiO_2}\left(\frac{W}{\rho}\right)_{TiO_2}}{Y_{Fe_3O_4}\left(\frac{W}{\rho}\right)_{Fe_3O_4} + Y_{TiO_2}\left(\frac{W}{\rho}\right)_{TiO_2} + \left(\frac{W}{\rho}\right)_{DIW}} \right) \quad (1)$$

Where Y is the ratio of the nanoparticles.

A variety of instruments and tools were employed for specific functions during the research, as detailed in Table 3.

SEM was Utilized to analyse the structural characteristics and dispersion of Fe_3O_4 and TiO_2. Stability evaluation incorporated diverse techniques, including rheological analysis, UV–Vis spectroscopy, heat conduction assessments, and direct visual observations, as illustrated in Fig. 2.

2.2. Magnetic field generation, method and control setup, optimized heat transfer efficiency

The current study adopts the methodology outlined by Adogbeji et al. [34], wherein the voltage was varied at 2 V, 4 V, 6 V, 8 V, and 12 V, while the frequency was adjusted across 40 Hz, 60 Hz, 80 Hz, 100 Hz, 500 Hz, and 1000 Hz. The duty cycle was consistently maintained at 50 %, with a phase shift of 90°. Sine, square, and triangular waveforms were utilized, with corresponding periods observed as 16.7 ms, 12.5 ms, 10.0 ms, and 20.0 ms. This approach effectively investigates the influence of magnetic field parameters on fluid dynamics and thermal performance.

The apparatus used to facilitate heat transfer in MHNFs comprises an advanced Digital Oscilloscope (IDS-2000 A series), a UNIT UT900E Signal Generator, a TS250 Signal Amplifier from Accel Instruments, magnetic coils (dimensions: 220 L × 46 W x 29D), a GM08 Magnetic Field Meter, and a connection hub. The magnetic coils, powered at either 12 V or 24 V DC with a maximum current consumption of 250 mA, receive their power supply through the signal amplifier. The oscilloscope monitors waveforms voltage and current from the amplifier, while the function generator adjusts waveform types (sine, square, triangular), frequency, period, and duty cycle.

The signal amplifier interfaces with a connection hub, facilitating the operation of four magnetic coils strategically positioned above the test section to cover all seven thermocouple stations Fig. 3. Magnetic field parameters, including waveform type and amplitude, are adjusted, and the system is stabilized before applying the magnetic field under continuous heat flux conditions.Fig. 4 illustrates, (a) the determination of viscosity and assessment of colloidal stability, and (b) the measurement of electrical conductivity and pH characteristics of the hybrid nanofluids.

2.3. UV–visible spectroscopy analysis for MHNFs

The UV–Vis spectroscopic analysis of Fe_3O_4/TiO_2 was performed following the same procedure outlined in our previous study Adogbeji et al., [33]., The Spectrophotometer was used at ambient conditions with Diw as the standard baseline. Each measurement was conducted in triplicate, and the averages were computed. The absorbance data for the MHNFs and the sedimentation factor were derived as per Eq. 2 from the earlier work [33].

$$\text{Percentage (SF)} = \left(\frac{\textit{Maximum absorbance} - \textit{Total average absorbance}}{\text{Maximum absorbance}} \right) \times 100 \quad (2)$$

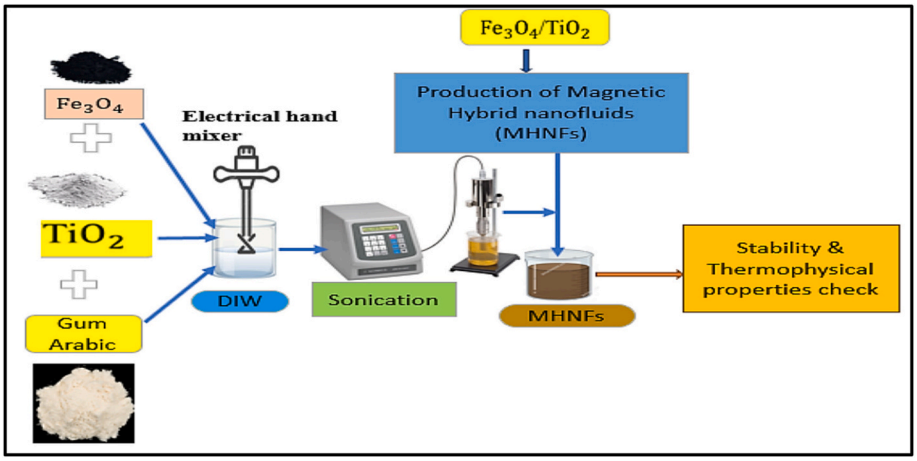

Fig. 1. Schematic process for preparation of MHNFs.

Table 3
The equipment and instruments used in the study.

Equipment/Instrument	Model/Manufacturer	Purpose	Specifications/Accuracy
Thermal Conductivity Analyzer	KD2 Pro, Decagon Devices Inc. (METER Group)	Measuring thermal conductivity (κ) of MHNFs	Range: 0.02–2.0 kW/m^2 Accuracy: ±10 %
pH Meter	Jenway 3510, Staffordshire, UK	Measuring pH levels of nanofluid samples	Range: −2 to 19.999; Accuracy: ±0.003
Conductivity Meter	CHAUVIN ARNOUX, C.A 10141, France	Measuring electrical conductivity of MHNFs	Accuracy: ±1 %
Temperature Range for Tests	–	Thermal conductivity and viscosity measurements	10 °C to 50 °C
Vibro-Viscometer	SV-10 A series, A&D, Tokyo, Japan	Measuring viscosity of MHNFs	Accuracy: ±1 %
UV–Visible Spectrophotometer	ONDA TOUCH UV-21 Spectrophotometer	Determining absorbance and sedimentation	Not specified
Scanning Electron Microscopy (SEM),	JEOL JEM-2100F, Tokyo, Japan	Examining nanoparticle morphology in dry state	Not specified

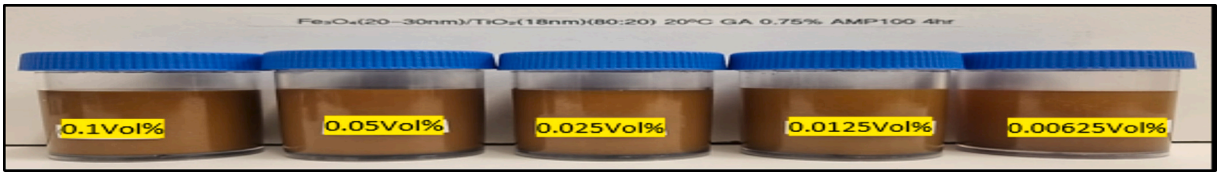

Fig. 2. Visualization of different volume fractions of **Fe_3O_4**/ **TiO_2** /DIW Magnetic Hybrid Nanofluid.

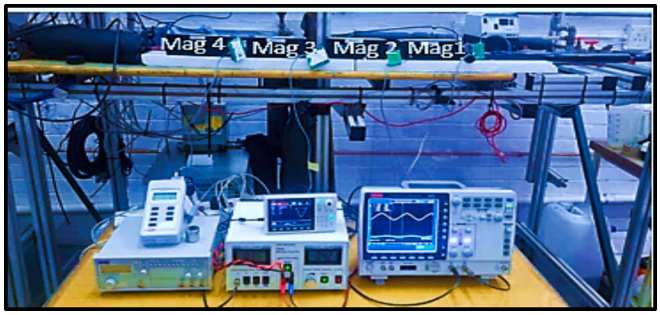

Fig. 3. Magnetic field generation and control setup.

2.4. Setup for evaluating electrical and thermal conductivity (TC) along with pH

The methodology to examine electrical and thermal conductivity, as well as pH, was based on the same setup and procedure as described in Adogbeji et al. [33]. The experimental configuration, including instrumentation for thermal conductivity analysis with a Controlled bath temperature, remained unchanged. Fluid characteristics such as electrical, thermal conductivity, and pH were examined continuously at temperatures of 5 °C intervals up to 50 °C. The same equipment and techniques were used to ensure consistency between this study and the prior investigation, thereby facilitating direct comparison of results.

2.5. Electrical conductivity (EC), pH and viscosity evaluation

The methodology for assessing viscosity, electrical conductivity, and pH of magnetic hybrid nanofluids follows the approach detailed in our previous study Adogbeji et al. [34], where the same equipment and procedures were used for these measurements. Viscosity measurements of Fe_3O_4/TiO_2 nanofluids and deionized water were evaluated in accordance with the previous study. The temperature was varied in 5 °C intervals, and the viscosity was recorded immediately after preparation and monitored over 24 h to examined nanofluids' homogeneity at different time intervals. Similarly, electrical conductivity and pH characteristics were measured in a manner consistent with our earlier work. The results from these tests are illustrated in Figs. 3a and b, with the data providing insight into the behavior of MHNFs under varying thermal conditions.

2.6. Uncertainty analysis of measured parameters

The approach outlined in [35]was utilized to estimate the uncertainty associated with key measured parameters, including dynamic viscosity (μ) and standard deviation (σ), by applying Eqs. (4) and (5). These uncertainties were determined with a 95 % confidence level. Instrument precision was assessed based on bias errors, which reflect the accuracy limitations specified by the equipment manufacturer. The uncertainty in viscosity measurements was found to be ±1.93 %, while that of electrical conductivity measurements was ±2.19 %.

$$U_\mu = \sqrt{\left(\frac{\Delta m}{m}\right)^2 + \left(\frac{\Delta V}{V}\right)^2 + \left(\frac{\Delta T}{T}\right)^2 + \left(\frac{\Delta \mu}{\mu}\right)^2} \quad (4)$$

Fig. 4. (a) Viscosity determination and stability assessment (b) measurement of electrical conductivity and pH characteristics.

(a)

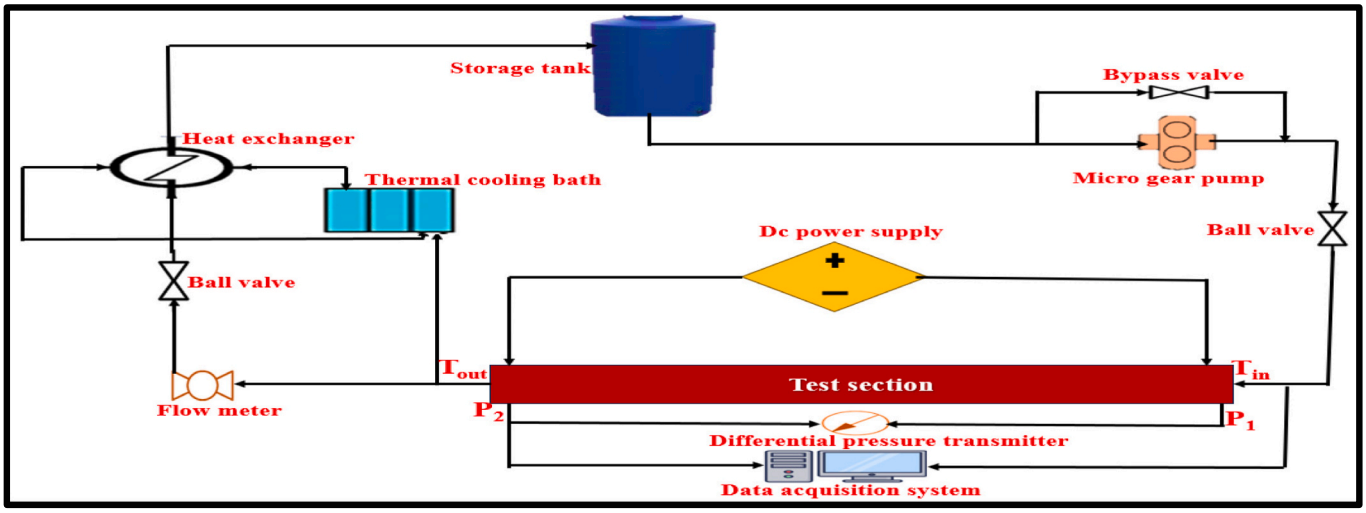

(b)

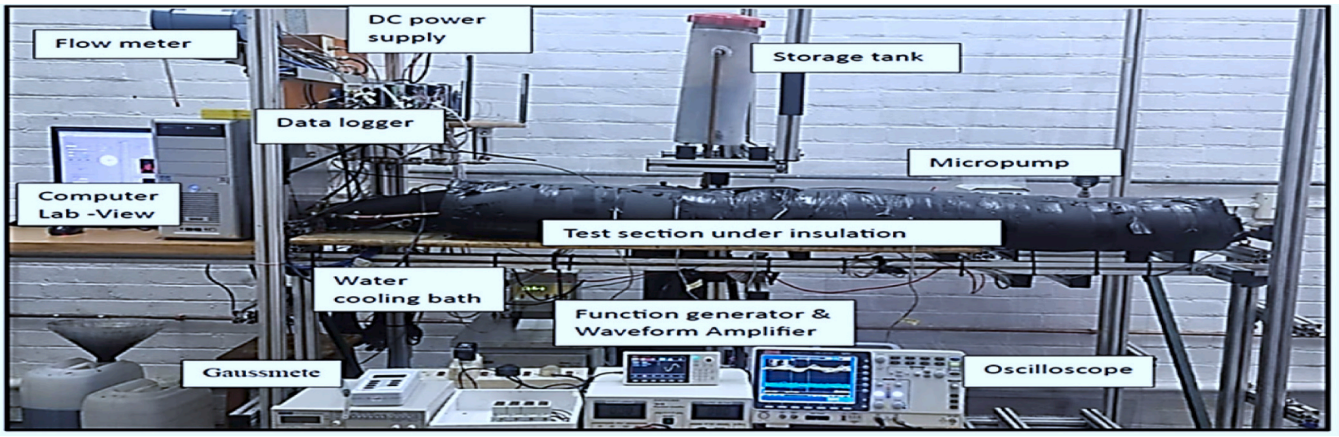

(c)

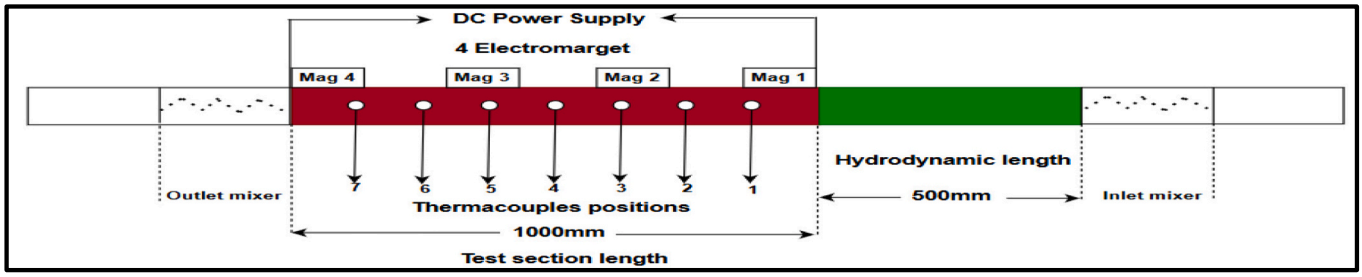

Fig. 5. (a) Test rig components (b) Pictural of test rig and magnetic equipment (c) Configuration of the experimental test section.

$$U_\sigma = \sqrt{\left(\frac{\Delta m}{m}\right)^2 + \left(\frac{\Delta V}{V}\right)^2 + \left(\frac{\Delta T}{T}\right)^2 + \left(\frac{\Delta \sigma}{\sigma}\right)^2} \quad (5)$$

2.7. Experimental configuration and approach for Analysing FCHT

Based on the setup described in Adogbeji et al. [34], Figs. 5a, b, and 5c show the experimental rig, which includes components such as a micro gear pump, pressure sensor, flow meter, test section, heat exchanger, thermocouples, DC power supply, and data acquisition system. The fluids are pumped through test rig, and their mass flow rate is evaluated. The nanofluid, heated at an inlet temperature of 20 °C, is cooled via the heat exchanger, with temperature and pressure monitored throughout.

In Fig. 5c, the test section consists of a 1550 mm long copper pipe (8 mm inner diameter, 9.5 mm outer diameter), with thermocouples placed at 130 mm intervals. A 200 W constantan wire maintains steady heat flux, powered by a direct current set to 180 V and 1.22 A. The test rig length is reduced to 1000 mm to ensure fully developed flow. Each experiment is repeated three times, and data is averaged for analysis.

The investigation of thermophysical properties for the magnetic hybrid nanofluids was conducted, focusing on key characteristics such as specific heat and density. These properties were calculated using the

model established by Pak and Cho [36], as defined in the following Eqs. (6) and (7).

Nanofluid density:

$$\rho_{nf} = (1-\varphi)\rho_{bf} + \varphi\rho_{np} \tag{6}$$

Nanofluid specific heat:

$$C_{pnf} = \frac{(1+\varphi)\rho_{bf}C_{pbf} + \varphi\rho_{np}C_{pnp}}{(1-\varphi)\rho_{bf} + \varphi\rho_{np}} \tag{7}$$

For the determination of specific heat and density Fe_3O_4/TiO_2 the models outlined in (8) and (9) [37].were applied.

Power supplied:

$$P = VI \tag{8}$$

Heat absorbed by fluid:

$$Q = \dot{m}c(T_O - T_i) \tag{9}$$

To assess convective heat transfer and the *Nu* at varying volumetric fractions, the energy stored in the fluid and the energy injected into the test rig were evaluated using the following relations 10 and 11. [38].

Local CHT coefficient:

$$\mathrm{h} = \frac{\mathrm{Q}}{A(t_w - t_b)} \tag{12}$$

Nusselt number:

$$\mathrm{Nu} = \frac{\mathrm{hD}_i}{\mathrm{k}} \tag{13}$$

Additionally, the study also accounted for the pressure losses due to viscosity in the test rig for both DIW and magnetic hybrid nanofluids. These results outcomes were juxtaposed with predicted frictional resistance values obtained using the relation presented in (14) [38], The parameters used during the experiments are listed in Table 4.

$$f = \frac{\Delta P}{\left(\frac{L}{D_i}\right)\left(\frac{\rho v^2}{2}\right)} \tag{14}$$

3. Experimental arrangement for forced convective heat transfer analysis and methodology

3.1. Nusselt number validation

Initial tests with DIW with range of flow conditions from *Re* 3200 to 55,000 were conducted prior to commencement with investigations of the CHT coefficients using nanofluids. The results obtained for the DIW were validated by comparison with equations specifically formulated for turbulent flows per Eqs. 15 and 16, and as outlined by Olivier and Meyer, [39], and Ghajar and Tam (1994) [37], respectively.

$$Nu = 0.026.Re^{0.8}.Pr^{0.385}.\left(\frac{x}{D}\right)^{-0.0054}\left(\frac{u}{u_w}\right)^{0.4} \tag{17}$$

$$3 \le \frac{x}{D} \le 192; Re\,7000 \le 49000; 4 \le Pr \le 34; 1.1 \le \frac{u}{u_w} \le 1.7$$

$$Nu = 0.026.Re^{0.788}.Pr^{\frac{1}{3}}.\left(\frac{u_b}{u_w}\right)^{0.4} \tag{18}$$

$3000 \le Re \le 17{,}800$ and $3.73 \le Pr \le 5.06$

From Fig. 6, the comparison of Nusselt numbers calculated using the experimental data with those predicted by Olivier and Meyer's correlation showed a mean discrepancy of 0.47 %, with a maximum variation of 6.6 % under the turbulent region. In like manner, the predictions derived from the Ghajar and Tam model exhibited an average difference of 3.4 %, reaching a maximum deviation of 10.5 % in the same flow regime. These findings demonstrated a strong agreement with the experimental results for deionized water, effectively confirming the reliability and accuracy of the experimental procedure.

Table 4
experimental conditions and parameters

Experimental conditions	specific ranges of key variables
Range of flow conditions (*Re*)	1000–8000
Thermal input	8.67kw/m^2
Geometric characteristics	9.5 mm External and 8 mm Internal diameter
Length of test rig	1000 mm
Temperature of nanofluid inlet	21 °C

3.2. Analysis of measurement uncertainty

The uncertainties associated with the experimental results were calculated at a 95 % confidence level using a methodology similar to that described by Ibrahim et al. [5] and Adogbeji et al. [40], which was adapted from the framework proposed by Dunn [41], as outlined in the following Eqs. 19,20 and 21.

Uncertainty estimates were carried out for both higher and lower Reynolds numbers, specifically 5000 and 1000, following a methodology analogous to that employed by Osman et al. [42] and Ibrahim [5]. At the higher Re of 5000, the deviations for the Nu, heat transfer coefficient (h), and Re were determined to be 6.8 %, 4.6 %, and 9 %, respectively. Conversely, at the lower *Re* of 1000, the uncertainties were 3.6 %, 5.3 %, and 7.5 % for *Nu*, h, and *Re*, respectively.

$$\frac{\delta Nu}{Nu} = \sqrt{\left(\frac{\partial h_{avg}}{h_{avg}}\right)^2 + \left(\frac{\partial D_h}{D_h}\right)^2 + \left(\frac{\partial k}{k}\right)^2} \tag{19}$$

$$\frac{\delta Re}{Re} = \sqrt{\left(\frac{\partial \rho}{\rho}\right)^2 + \left(\frac{\partial V}{V}\right)^2 + \left(\frac{\partial D_h}{D_h}\right)^2 + \left(\frac{\partial \mu}{\mu}\right)^2} \tag{20}$$

$$\partial h(x) = \sqrt{\left(\frac{\partial h(x)}{\partial \dot{q}}\delta\dot{q}\right)^2 + \left(\frac{\partial h(x)}{\partial T_s}\delta T_s\right)^2 + \left(\frac{\partial h(x)}{\partial T_m}\delta T_m\right)^2} \tag{21}$$

3.3. Morphology analysis of nanoparticles and thermophysical characteristics of MHNFs

The structural properties and stability of nanofluids comprising Fe_3O_4 with varying ratio of TiO_2 were analyzed through SEM, as shown in Fig. 7. The SEM pictures were obtained at a 100,000× magnification, using 2.0 kV and a speed of 9 μm/s. The SEM micrograph of Fe_3O_4 exhibited a non-uniform dispersion of nanosheets with varying sizes, while TiO_2 nanoparticles were observed to have predominantly spherical morphology. The SEM image of the hybrid Fe_3O_4—TiO_2 nanofluid demonstrated effective dispersion, suggesting the formation of a stable suspension. However, Fe_3O_4 particles appeared more prominent

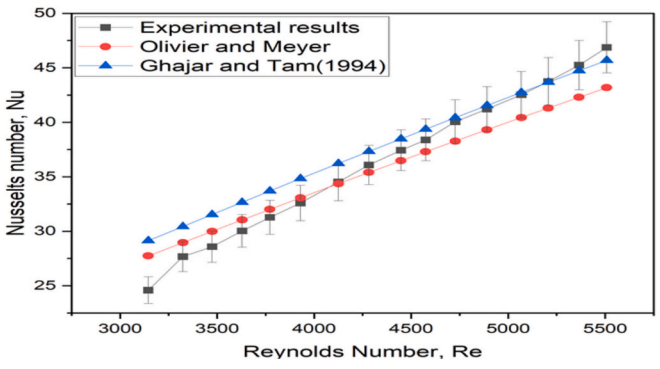

Fig. 6. Results for deionized water testing to validate the experimental setup.

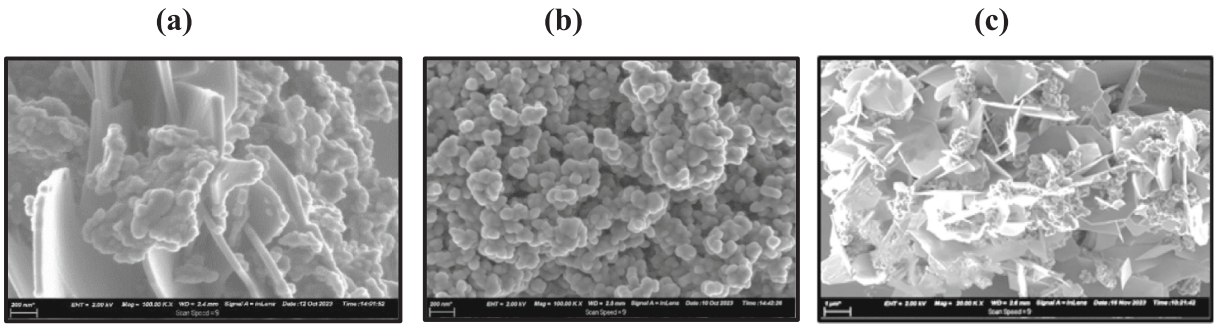

Fig. 7. Morphology analysis: (a) Fe_3O_4 and (b) TiO_2; (c) hybrid Fe_3O_4—TiO_2.

compared to their TiO_2 counterparts.

The viscosity stability of these nanofluids was assessed at a temperature of 30 °C over a duration of 10 h, following the approach outlined in previous studies by Giwa et al. [43], and Osman et al. [44]. The stability outcomes are represented in Fig. 8a. A 30-day visual inspection revealed negligible sedimentation of the fluids with volume ratio of 0.00625 %, 0.0125 %, and 0.025 %, whereas minor settling was observed at a volume fraction of 0.05 %. In contrary, fluids with a volume ratio of 0.1 % exhibited noticeable sedimentation.

The assessment of nanofluid stability carried out using UV–Vis spectrophotometry, adhering to the principles of Beer- Beer-Lambert's law [44,45], This method highlighted a clear association between the absorbance values of Fe_3O_4—TiO_2 and their nanoparticle volume ratio, as illustrated in Fig. 8b. The findings of Chakraborty et al. [46], demonstrated that the stabilization properties of nanofluids could be quantitatively determined by observing changes in optical absorption trends over time. A decrease in absorbance signals instability, which is indicative that the nanoparticles are beginning to separate from the suspension. The analysis revealed that lower absorption intensities were associated with reduced nanoparticle concentrations, which corresponded to sedimentation rates. Throughout a 30-day monitoring phase, notable sedimentation was recorded for fluids with 0.1 % volumetric concentration, with sedimentation factor (SF) values measured as 11.61 % for 0.1 vol%, 10.68 % for 0.05 vol%, 10.24 % for 0.025 vol%, 9.82 % for 0.0125 vol%, and the lowest value of 8.89 % for 0.00625 vol%.

Conversely, nanofluids with particle loadings of 0.00625 %, 0.0125 %, and 0.025 % exhibited significant steadiness over time 30 days. The minor instability identified for the 0.05 % particle fraction indicates the possible requirement for fine-tuning the dispersing agents, especially at elevated particle concentrations. This decreasing trend indicates that at elevated particle concentrations lead to greater sedimentation, causing the nanofluid to be less stable over time. Conversely, lower concentrations slow the sedimentation rate thus improving the stability of the nanofluid and ensuring a more homogeneous dispersion of particles [3],.

The variation in the viscosity of Fe_3O_4—TiO_2/DIW with the range of temperature of 10 °C to 50 °C is illustrated in Fig. 9a, indicating a reduction in viscosity with rising temperature. Fig. 9b and c display increases in with the EC and TC with higher nanoparticle volumetric fractions, consistent with findings by Zadkhast et al. [47] and Oraon et al. [48]. Furthermore, Fig. 9d reveals a decrease in the pH of Fe_3O_4—TiO_2as temperature increases. Elevated nanoparticle (n_p) amplifies the pH, reducing it, signifying increased acidity. In contrast, DI water maintains a nearly stable pH of approximately 7, highlighting the significant impact of n_p on the Fe_3O_4—TiO_2/DIW pH. These patterns agreed with earlier investigations by Krishnan et al. [49] and Giwa et al. [43] underscoring the Interwoven dynamics between the thermophysical characteristics of nanofluids, concentration, and temperature.

4. Findings and analysis

4.1. Variation of CHT with nanoparticle volume fractions

Fig. 10 demonstrates the effect of varying volume fractions on the CHT coefficient for Fe_3O_4/TiO_2 nanofluids at different *Re*. The percentage improvements in the CHT coefficient, compared to DIW, follow a noticeable trend. In our previous study (Adogbeji et al. [34],*We* reported an enhancement of 16 % at a volume fraction of 0.1 %. As the nanoparticle concentration decreases, the enhancements continue to rise, with a peak of approximately 20.36 % at a 0.05 % volume fraction. Further reductions in concentration led to substantial augmentation, with the maximum enhancement of around 27.28 % at a 0.0125 % volume fraction. Even at the lowest concentration of 0.00625 %, the CHT coefficient exhibited an increase of about 22.47 %. These results,

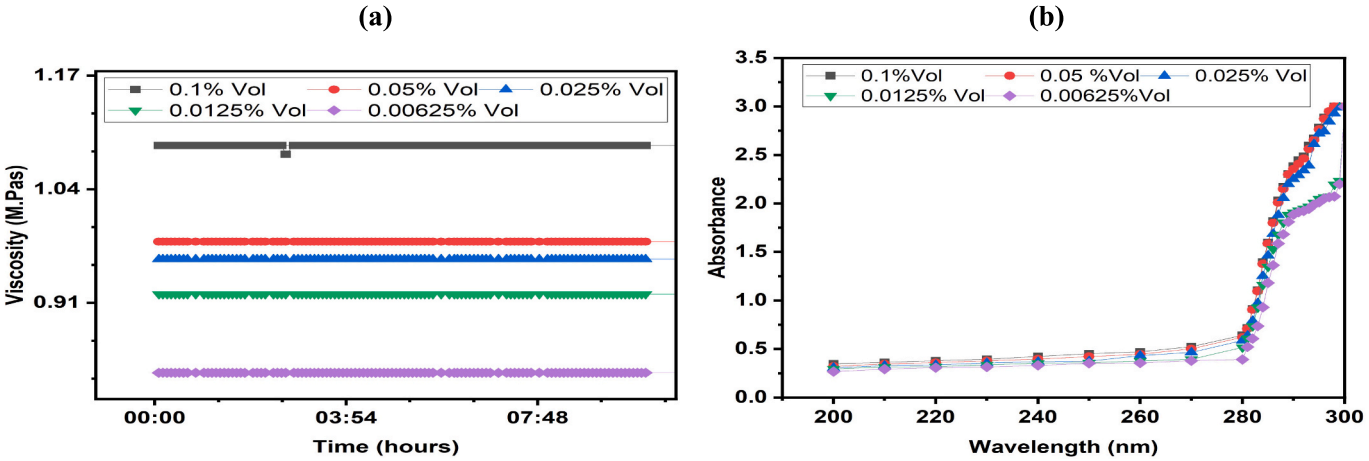

Fig. 8. (a) Evolution of Fe_3O_4—TiO_2 stability with time (b) Influence of Fe_3O_4—TiO_2 concentration on optical absorbance across various wavelengths.

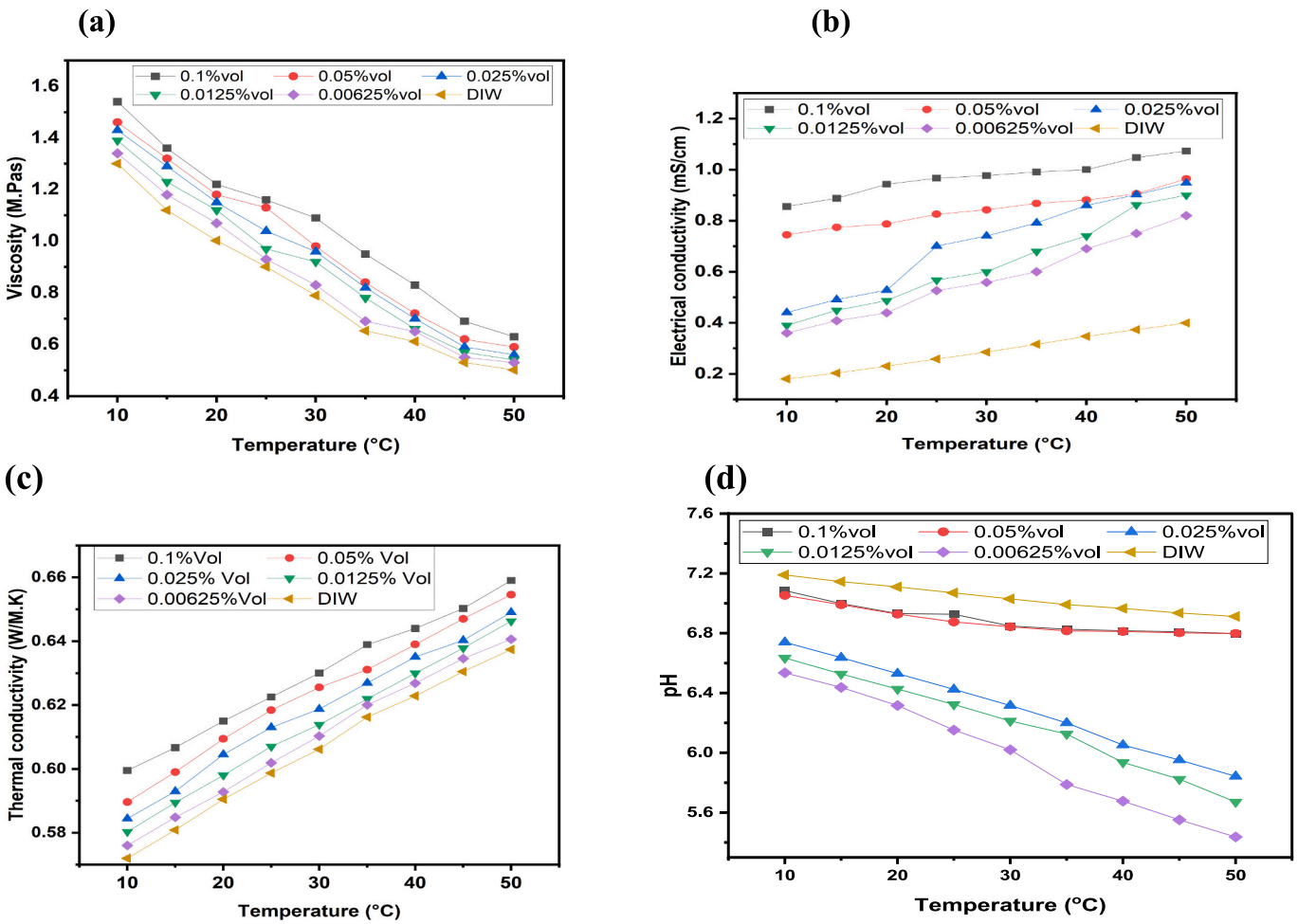

Fig. 9. (a) Temperature-induced changes in viscosity, (b) Influence of temperature on EC, (c) Effect of temperature on TC, and (d) Temperature-driven fluctuations in pH for various nanoparticle volume fractions.

derived from our earlier work, further underscore the positive impact of Fe_3O_4/TiO_2 hybrid nanofluids on heat transfer performance at different concentrations, emphasizing the consistency and reproducibility of our findings.

4.2. *Effect of magnetic waveform placement on CHT*

Placing the magnetic waveform (M_{wf}) along the test section can substantially affect heat transfer enhancement, entropy generation, and thermal performance in turbulent flow conditions. Researchers can optimize these thermal processes by carefully selecting the waveform's placement and Magnetic field strength (MFS). Fig. 11 illustrates several scenarios: **Case I**, which has no magnetic field, serves as a reference point for comparison, while **Cases II** through **IV** present various magnetic field configurations. These cases showcase the different effects on heat transfer, entropy production, and thermal performance. Effectively controlling the magnetic waveform's positioning is essential for achieving optimal heat transfer in real-world applications.

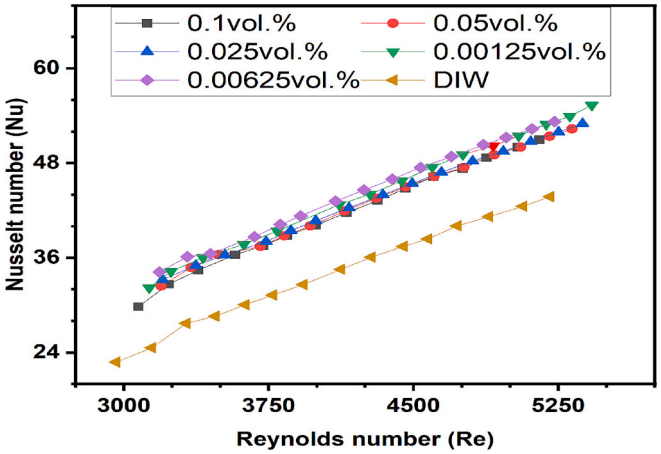

Fig. 10. Impact of volumetric ratio on CHT coefficient enhancement.

Fig. 12a illustrates optimization analysis of frequency and MFS, As reported in Adogbeji et al., the MSF with different waveforms (sine, square, and triangular) in electromagnetic heat transfer systems was analyzed. The study found that as the frequency increased from 40 Hz to 1000 Hz, there was a consistent rise in MFS, confirming the positive relationship between frequency and the effect on heat transfer. The results showed that the Sine wave constantly generated maximum MFS effects compared to the triangular and square waves at higher frequencies. Notably, a convergence point was observed at 40 Hz and 60 Hz, where all three waveforms intersected, highlighting the significant to optimized field parameters for improving CHT. The study also demonstrated a direct relationship between voltage and MFS, as seen in Fig. 12b. As voltage levels increased, the MFS correspondingly increased, with the Sine waveform consistently producing the highest MSF. The triangular followed, while the square generated the lest MFS. At 4 V, a convergence point was observed, emphasizing that the field should be controlled. These findings, as presented in Adogbeji et al., are

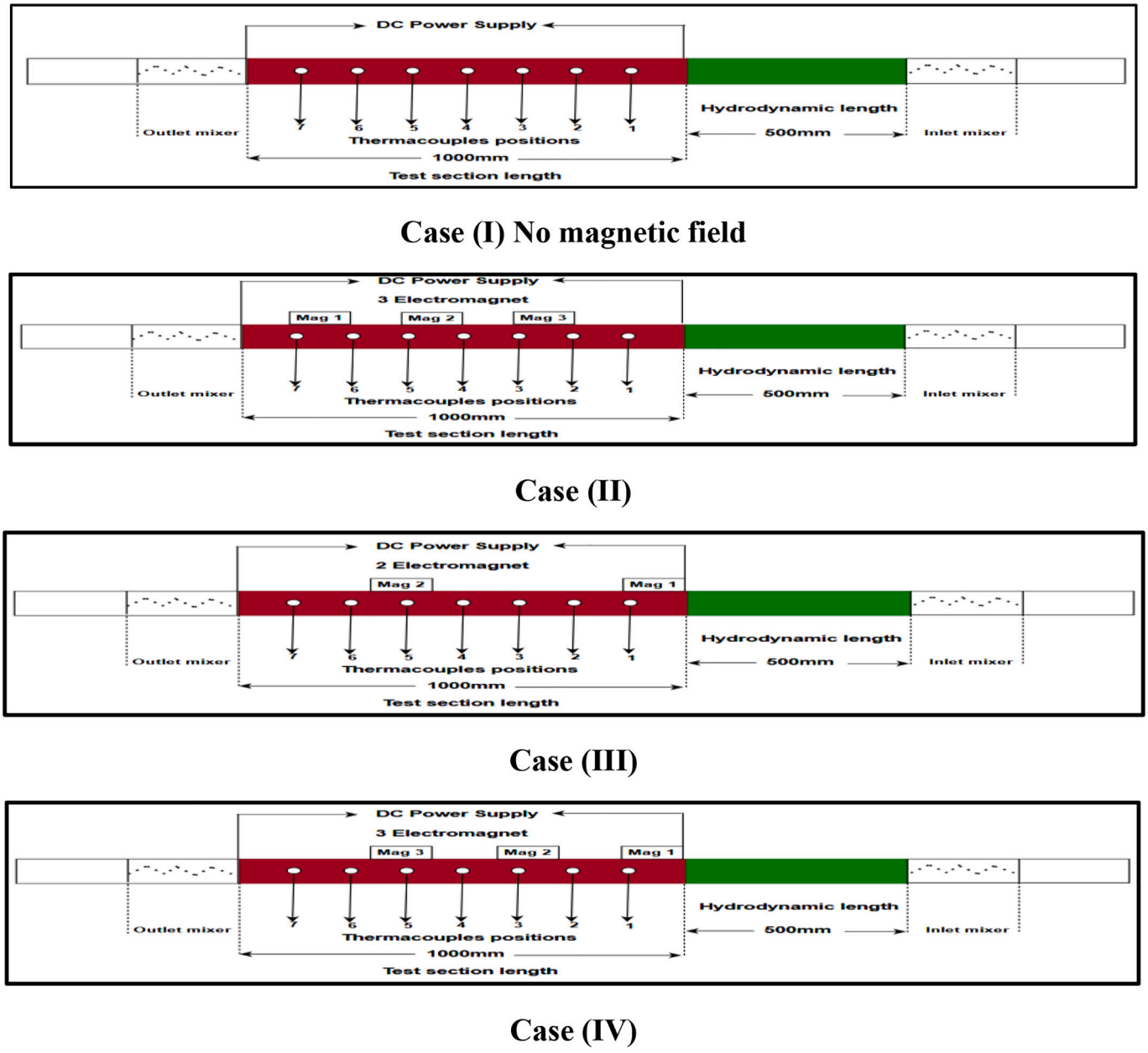

Fig. 11. Diagrammatic illustrations of various magnetic field positions along the test rig under investigation

critical for optimizing thermal management devices that leverage the effects of MF on heat exchange.

The results depicted in Fig. 13**a, b,** and **c** for **Case (II)** are based on findings from our earlier study (Adogbeji et al., [34],), which demonstrated significant heat transfer enhancement when waveforms were applied. At a volume concentration of 0.0125 %, the heat transfer enhancements for sine, square, and triangular waves were 18.5 %, 16.2 %, and 15.9 %, respectively, compared to absent of field. Similarly, at 0.00625 % concentration, the enhancements were 14.1 %, 13.5 %, and 13.2 %, respectively. These previously published results have been incorporated into this study to facilitate a comparative evaluation with other cases, underscoring the impact of field placement on heat augmentation systems.

Fig. 14 **a, b**, and **c,** along with **Case (III)**, collectively demonstrate the significant impact of MF waves on enhancing heat exchange in the fluid. When MF waves are applied at different volume fractions (0.1 %, 0.05 %, 0.025 %, 0.0125 %, and 0.00625 %), they consistently improve heat exchange efficiency compared to conditions with and absent of magnetic field. However, an intriguing observation arises when comparing conditions with and absent of magnetic field at the same volumetric ratio with absent of field, there is a consistent heat transfer enhancement. This could be attributed to the influence of the magnetic field positioning at the beginning of the thermally developed area of the test section as illustrated in Fig. 11 **Case (III),** followed by demagnetization due to the distance between the first and second magnetic fields, likely contributing to fluctuations in heat augmentation. Particularly at lowest volumetric fractions, such as 0.00625 %, the presence of a magnetic field results in more substantial enhancements compared to when no magnetic field waves are applied, suggesting a nuanced relationship between magnetic field positioning and heat transfer enhancement. Furthermore, the comparison with DIW demonstrates the pronounced impact of magnetic field waveforms in improving fluid flow behavior and enhancing heat transfer performance across all volumetric ratio. The findings emphasize that strategic optimization of magnetic field placement can significantly enhance heat dissipation, presenting promising opportunities for advancing thermal regulation systems and

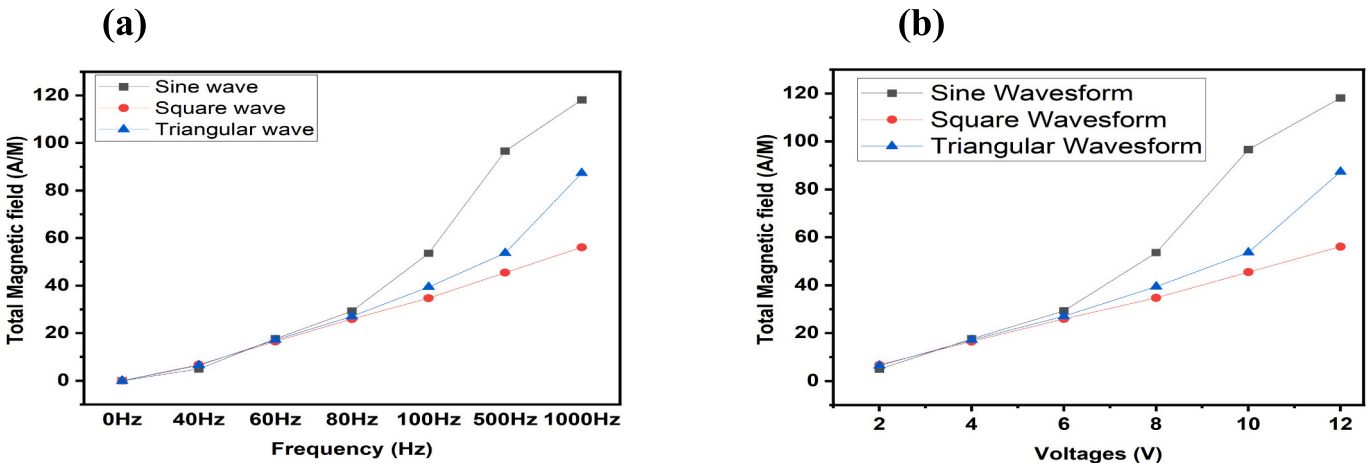

Fig. 12. (a) Optimization analysis of frequency and MFS among various waveforms in electromagnetic heat transfer systems (b) Optimization analysis of voltages and MFS across various waveforms in electromagnetic heat exchange systems

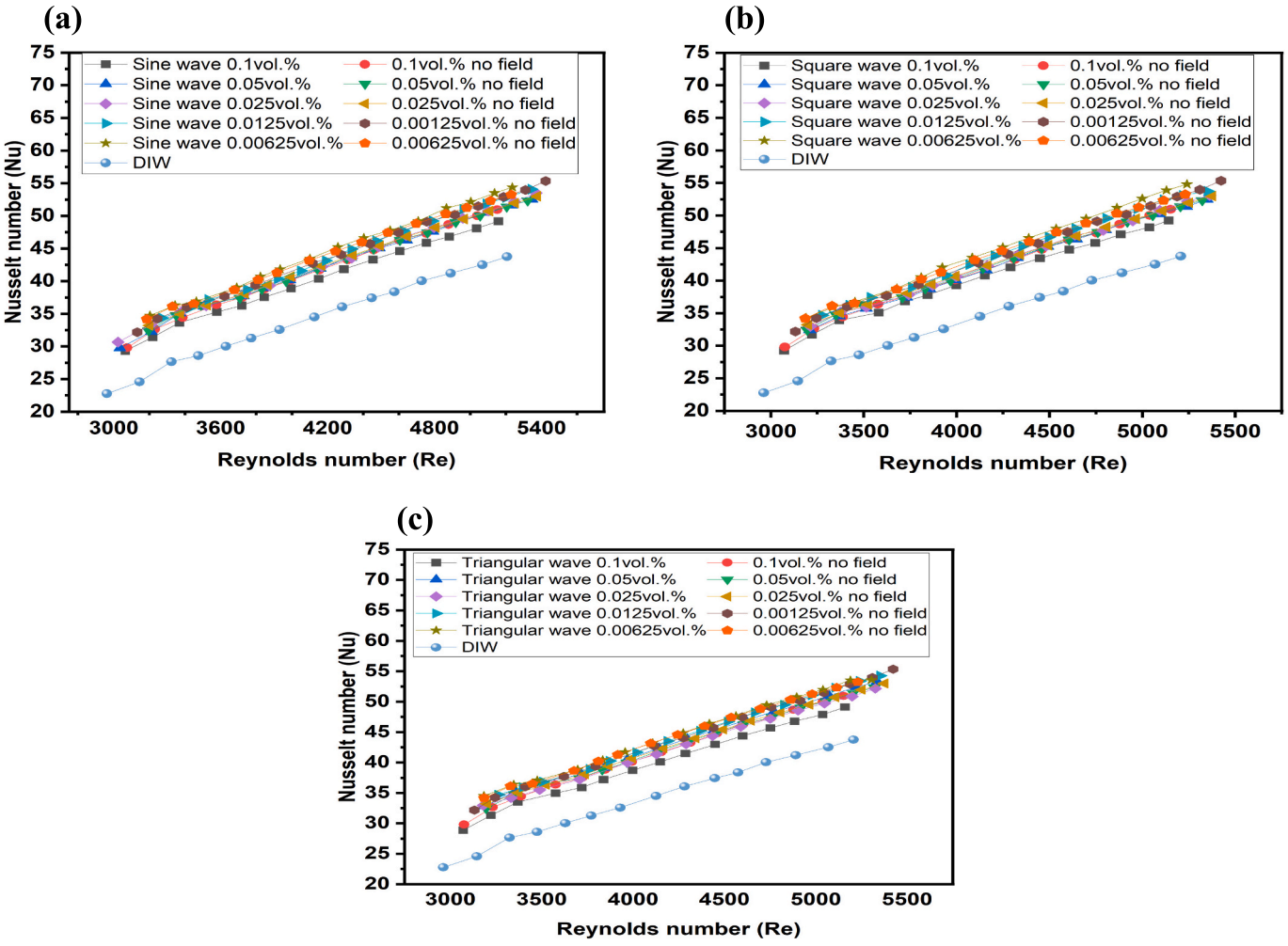

Fig. 13. Heat transfer enhancement with case (ii) magnetic field (a) sine (b) square and (c)triangular waves at different volume fractions

fluid-based heat exchange application **(b)**

Fig. 15**a, b**, and **c**, along with **Case (IV),** collectively demonstrate the significant impact of MF waves on enhancing heat exchange in the fluid. When MF waves are applied at different volume fractions (0.1 %, 0.05 %, 0.025 %, 0.0125 %, and 0.00625 %), they consistently improve heat transfer efficiency. In **Case IV, depicted in** Fig. 11, the thermocouple is positioned at the end of the thermally developed region where the electromagnetic field is applied, allowing us to observe the effect on the heat transfer coefficient specifically in this region. However, an intriguing observation arises when comparing conditions with and with and absent of magnetic field at the same volumetric fraction. Interestingly, the highest enhancement under this case was observed at

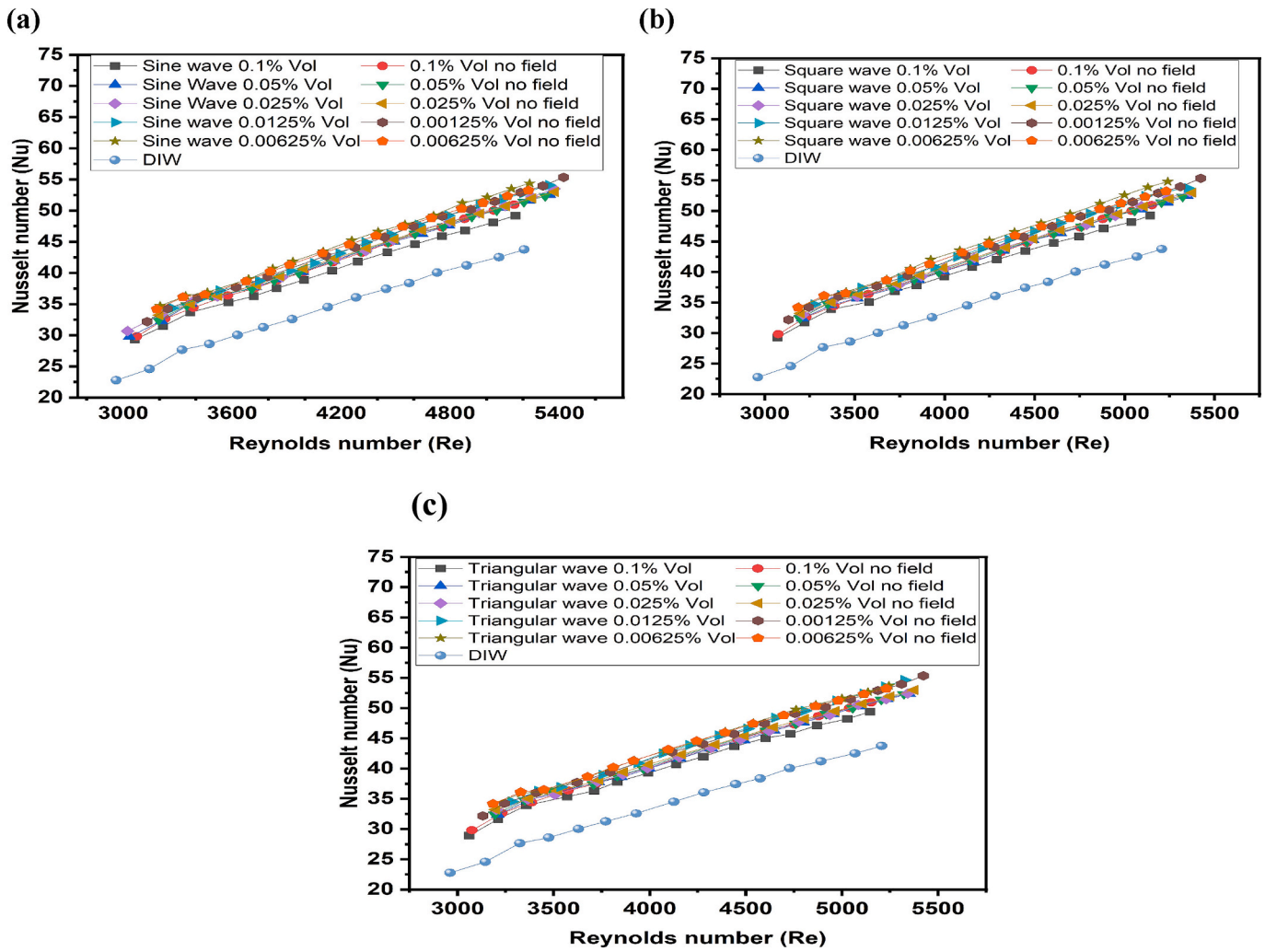

Fig. 14. Heat transfer enhancement with case (III) magnetic field (MF) (a) sine waves (b) square waves and (c) triangular waves at different volume fractions.

volumetric fractions of 0.00625 vol, 0.0125 vol, and 0.1 vol without a magnetic field across all waveform types. However, at a volumetric fraction of 0.025 vol, enhancement was noticed across all waveform types, more than in the case of no magnetic field. This behavior could be attributed to several factors. One possible explanation is that at lower volume fractions, the presence of the magnetic field produces a more substantial impact changes in the fluid dynamics and heat transfer characteristics, leading to enhanced heat transfer. Additionally, the positioning of the thermocouple at the end of the thermally developed region allows for a more accurate measurement of the heat transfer coefficient influenced by the magnetic field. Furthermore, the behavior observed at 0.05 vol and 0.025 vol might be associated with a particular dynamic involving the field and the nanofluid at this volumetric ratio, resulting in enhanced heat exchange despite the presence of a MF.

Fig. 16 illustrates significant variations in the CHT coefficient enhancement across different volume fractions, waveforms, and cases of Fe_3O_4/TiO_2 nanofluid. A rise in concentration leads to a reduction in enhancement in the CHT coefficient, with notable improvements observed particularly at lower volume fractions. At 0.00625 Vol, for instance, the CHT coefficients for sine wave **Case IV**, square wave **Case IV**, and triangular wave **Case IV** are 22.97 %, 25.28 %, and 22.44 %, respectively, compared to the base case value of 22.4 %. However, **Case IV** generally exhibits lower enhancement compared to other cases in all waveforms, possibly due to the positioning of the MF along the test rig, as depicted **in** Fig. 11 **Case (IV).** Conversely, in **Case III**, Fe_3O_4/TiO_2 nanofluid without a MF shows more enhancement from 0.1 Vol to 0.0125 Vol, except for at 0.00625 Vol where Square Waves demonstrate the highest enhancement at 25.28 %, followed by Sine Waves at 24.21 % and Triangular Waves at 22.81 % over no MF. This could be attributed to the influence of the MF positioning at the beginning of the thermally developed area of the test section, followed by demagnetization due to the distance between the first and second magnetic fields, likely contributing to fluctuations in heat augmentation. Square Wave cases demonstrate the highest enhancement percentages among the waveform cases, consistently outperforming sine and triangular wave cases. For instance, at 0.0125 Vol, the enhancement percentages for square wave **Case II** are 28.21 %, while for Sine wave **Case II**, it's 27.87 %. This could be attributed to the influence of the MF positioning from the beginning of the thermally developed area of the test section to almost the end of the test section, as illustrated in Fig. 11 **case (II)**, showing that the magnetic particles are homogeneously dispersed within the fluid during the flow, thereby causing improved enhancement along the test section. Moreover, at higher volume fractions, square Wave cases exhibit substantial enhancement compared to other waveforms. For example, at 0.1 Vol, the CHT coefficients for square wave **Case III** and triangular wave **Case III** are 12.58 and 12.95, respectively, while for Sine wave **Case III**, it's 12.42. However, at higher volume fractions (0.1 % Vol), the percentage enhancement in heat transfer generally decreases across all waveform types compared to the control condition without a magnetic field. This suggests a concentration-dependent behavior of the nanofluid, potentially influenced by factors such as particle distribution and agglomeration that the applied magnetic field helps to amplify.

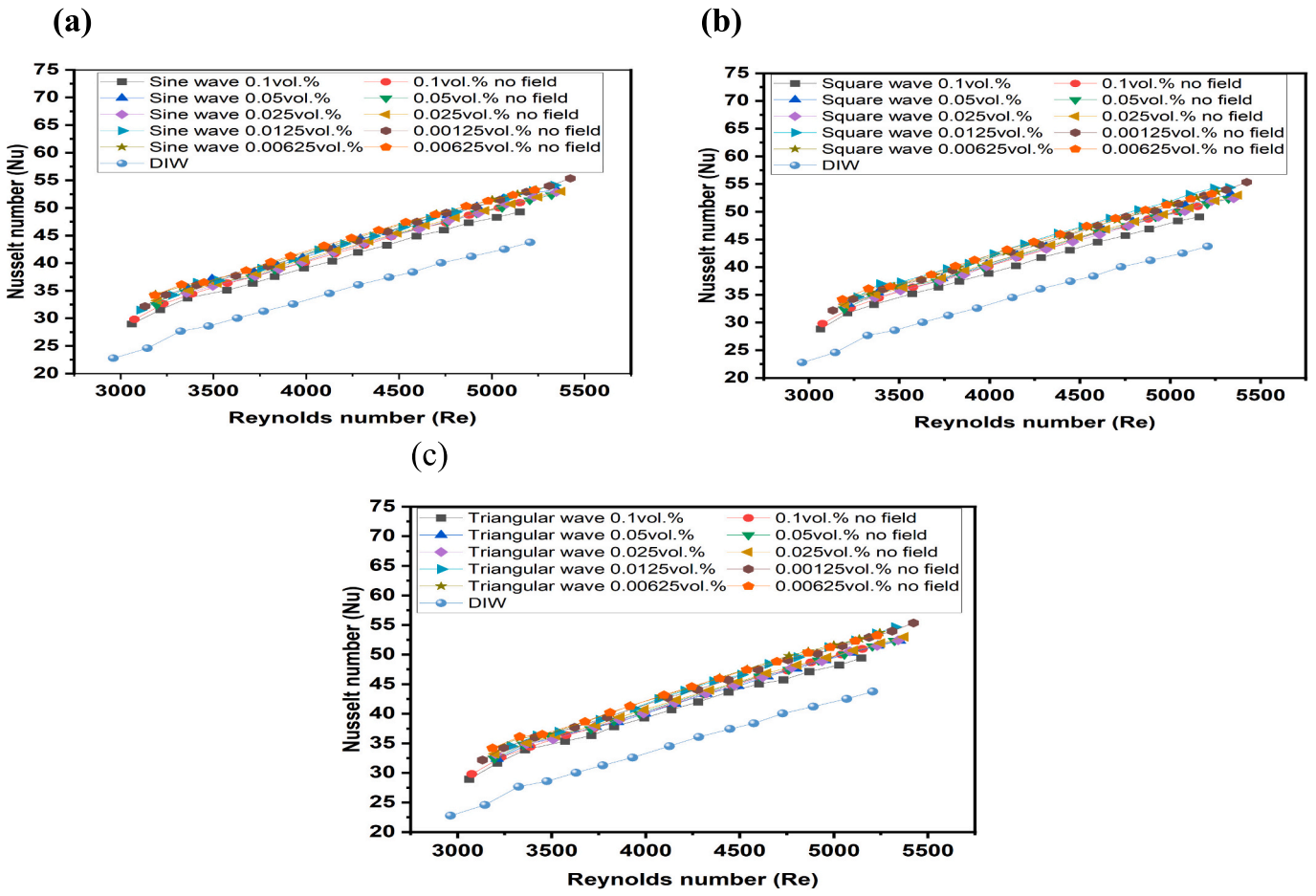

Fig. 15. Heat transfer enhancement with case (IV) magnetic field (a) sine wave (b) square waves and (c) triangular waves at different volume fractions

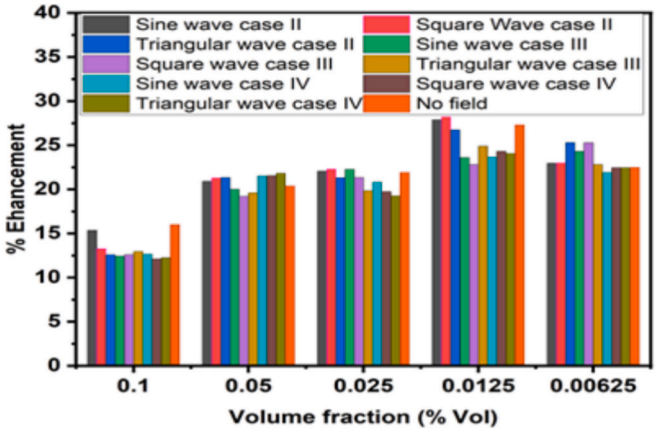

Fig. 16. Analysis of percentage enhancement of heat transfer across various waveforms and magnetic positions with varying volume fractions.

Consequently, increasing the volume fraction beyond a certain threshold may not lead to substantial improvements in heat transfer augmentation, even with the application of a magnetic field. It's important to note that the choice of waveform also impacts the enhancement, with square wave cases generally yielding the best results. However, square wave **Case III** also presents competitive enhancement values, showcasing its effectiveness in certain scenarios. Overall, the selection of the optimal case for maximizing heat transfer enhancement depends on various factors such as volume fraction, waveform characteristics, and specific application requirements. Therefore, a comprehensive understanding of each case's performance is essential for optimizing thermal management systems and fluid-based heat transfer processes.

Figs. 18(a), (b), and (c), Figs. 19(a), (b), and (c), Figs. 20(a), (b), and (c) represent **Case II, Case III,** and **Case IV**, respectively while Fig. 17 represent **Case I** no magnetic field, for magnetic hybrid nanofluids under varying conditions with a concentration ranging from 0.1 wt% to 0.000625 wt% and different waveforms at varying velocities, depicting the CHT behavior. Comparing the heat transfer coefficient (h_{avg}) values obtained with the impact of square, triangular, and sine waves, for **Case II, Case III,** and **Case IV**, as well as in the absence of a magnetic field across different volumetric fractions and velocities, reveals intriguing trends. At a volumetric fraction of 0.1 %, the CHT coefficient remains relatively consistent under sine waves for all cases, ranging from 3755 W/m^2 K to 3855 W/m^2 K at a velocity of 0.63 m/s, while without a magnetic field at the same velocity, the average heat transfer (h_{avg}) is higher at 3889 W/m^2 K. The same trend is observed in triangular and square waves throughout the various cases. The discrepancy in CHT coefficients between cases with and absence of the magnetic field at a volumetric fraction of 0.1 % can be attributed to several factors, including nanoparticle alignment, agglomeration, fluid dynamics alterations, and changes in suspension stability induced by the magnetic field. Similarly, at lowest volumetric fractions of 0.05 % and 0.025 %, h_{avg} values fluctuate within a narrow range for both conditions, suggesting minimal impact from the implementation of magnetic waveforms. Moving to lowest volumetric fractions of 0.0125 % and 0.00625 %, a slight divergence in h_{avg} values is observed between triangular, square, and sine waves for the three cases, with higher h_{avg} values consistently under sine wave conditions compared to no magnetic field conditions. The observed divergence suggests a significant influence of

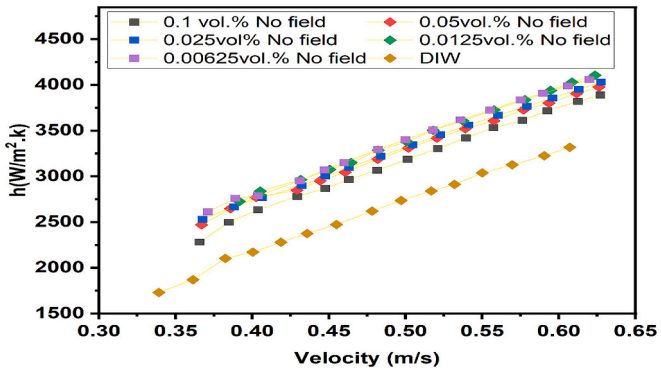

Fig. 17. Comparison of thermal performance metrics: magnetic hybrid nanofluids vs. deionized water across varying velocities and concentrations in the absence of magnetic fields Case I

the magnetic field on Fe_3O_4/TiO_2nanoparticle suspension at these lower volumetric fractions, potentially due to enhanced nanoparticle alignment, dispersion, and fluid flow alterations induced by the magnetic field. Overall, while applying magnetic waves may slightly influence CHT behavior in MHNFs, nanoparticle volume fraction and dispersion remain the dominant factors determining heat transfer efficiency. These results highlight the intricate relationship among nanoparticle concentration, fluid behavior, and external influences in heat transfer mechanisms., emphasizing the need for further research to optimize such systems.

4.3. Pressure drop

The frictional resistance of MHNF nanofluids through the test section is evaluated across a range of concentrations and flow rates. As illustrated in Fig. 21, under conditions where no magnetic field is present (referred to as **Case I**), the calculated friction factor for the MHNFs nanofluids is analyzed. According to theoretical expectations outlined in **Eq.** (14), the friction factor of MHNFs nanofluids is anticipated to rise because of viscous drag and density gradient. The observed results align with the anticipation, demonstrating an increase in the friction factor with higher MHNFs nanoparticle concentrations and a decrease with increasing flow velocity. This behavior is typical for fluid flow in straight tubes.

In Figs. 22**a, b**, and **c,** Figs. 23**a, b**, and **c,** and Figs. 24**a, b**, and **c**, which represent **Case II, III**, and **IV,** respectively, under the impact of magnetic waveforms, the pressure drop is shown as a function of flow velocity at different volume concentrations. The experimental data reveal the behavior of Fe_3O_4/TiO_2/DIW within the turbulent forced convection region, where multiple factors such as nanoparticle concentration, viscous drag effects, and flow dynamics play a role. The results demonstrate that increasing the nanoparticle concentration leads to a noticeable increase in the frictional resistance, with this trend becoming more prominent at higher concentrations, indicating that the

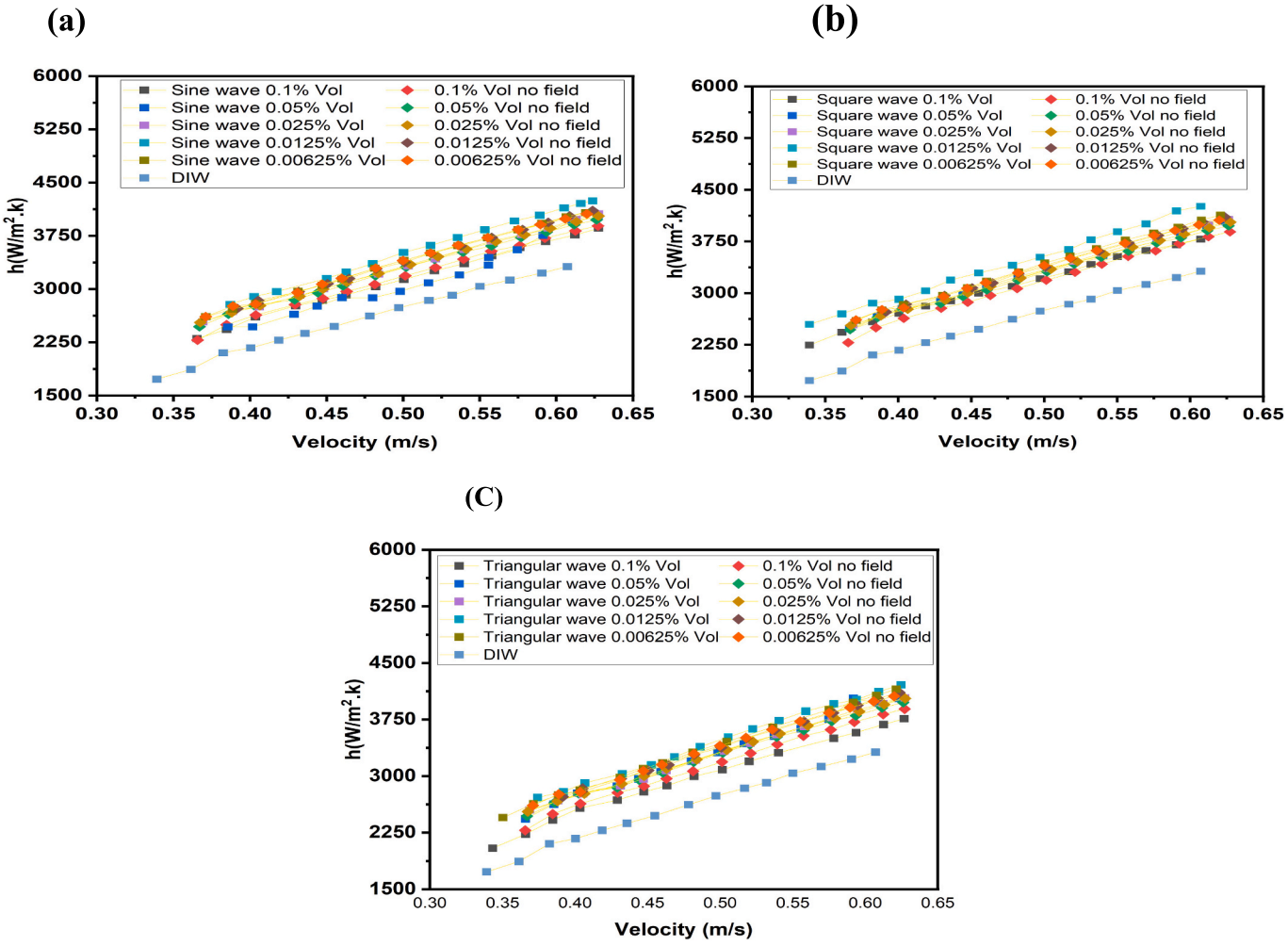

Fig. 18. Comparative analysis of heat transfer coefficients, magnetic hybrid nanofluids vs. deionized water across varying velocities and concentrations with magnetic waves and in the absence of magnetic fields Case II (a) Sine waves (b) Square waves (c) Triangular waves.

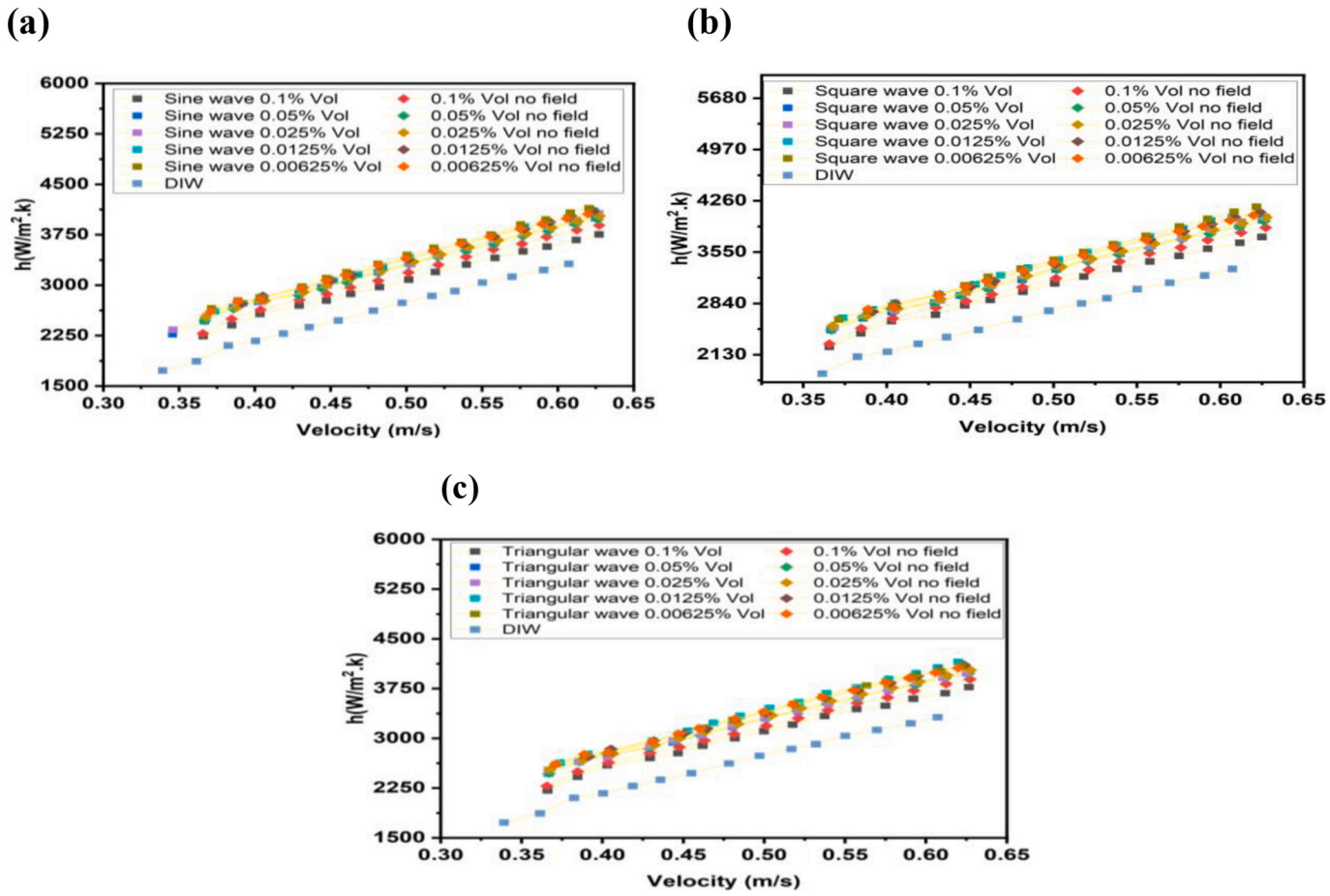

Fig. 19. Comparative analysis of heat transfer coefficients, magnetic hybrid nanofluids vs. deionized water across varying velocities and concentrations with magnetic waves and in the absence of magnetic fields Case III. (a) Sine waves (b) Square waves and (c) Triangular wave

nanofluid concentration directly impacts hydraulic resistance. Furthermore, the interplay between frictional resistance and flow velocity shows a linear reduction across all concentrations. This trend is consistent across all experimental cases. Interestingly, the pressure drop behavior at lower concentrations (0.00625 % and 0.0125 %) resembles that of DIW, suggesting that while flow velocity is the key factor, the presence of nanoparticles amplifies the pressure drop. These observations are consistent with earlier studies, such as those by Sadeghinezhad et al. [38,50] and Sundar [51].

4.4. Analysis of thermal performance factor (TPF) and its relationship with nanofluid concentration

To accurately assess the CHT and *Nu* in a system, it is essential to ascertain the thermophysical characteristics of the nanofluid. These properties, in conjunction with empirical data on frictional losses, facilitate the computation of a thermal efficiency metric for the system. The thermal efficiency metric (η) is defined in accordance with established guidelines [52]

$$\eta = \left(\frac{\left(\frac{Nu_{nf}}{Nu_{bf}} \right)}{\left(\frac{f_{nf}}{f_{bf}} \right)^{\frac{1}{3}}} \right) \tag{22}$$

Fig. 25 illustrates the thermal performance factor (TPF) for various magnetic hybrid nanofluid concentrations with no magnetic field. Notably, for volumetric ratio of 0.00625 wt% and 0.1 wt%, the thermal performance factor of Fe_3O_4/TiO_2. Surprisingly, the data reveal that a volume fraction of 0.0125 % leads to the most efficient heat exchange performance, contrary to the expectation that higher volumetric ratio would correlate with superior thermal performance [25]. This unexpected finding suggests that even a lower concentration of nanoparticles in the fluid can significantly enhance heat transfer. This result shows that increased thermal conductivity of a higher volume fraction does not necessarily contribute to a higher thermal performance factor. The trend indicates a reduction in the thermal performance factor ratio as velocity increases across all volume fractions. The implications for thermal management are profound, emphasizing the critical importance of optimizing nanoparticle volume fraction to achieve maximal thermal performance. This optimal volume fraction can be strategically utilized to enhance performance and increase energy efficiency in practical applications where maximizing heat transfer efficiency is paramount, such as in heat exchangers or cooling systems. However, achieving this optimal volume fraction requires careful consideration of various factors, including particle agglomeration, viscosity effects, interfacial resistance, thermal conductivity saturation, and nanoparticle distribution. By meticulously tuning nanoparticle volume fraction, engineers and researchers can unlock improved thermal performance and optimize thermal management systems for enhanced efficiency and effectiveness.

4.5. Impact of magnetic field positioning and waveforms on thermal performance factors in magnetic hybrid nanofluids

The thermal performance factor and its relationship with magnetic field positioning were examined, particularly focusing on the effect of different waveforms. Notably, concentrations of 0.00625 wt% and 0.1

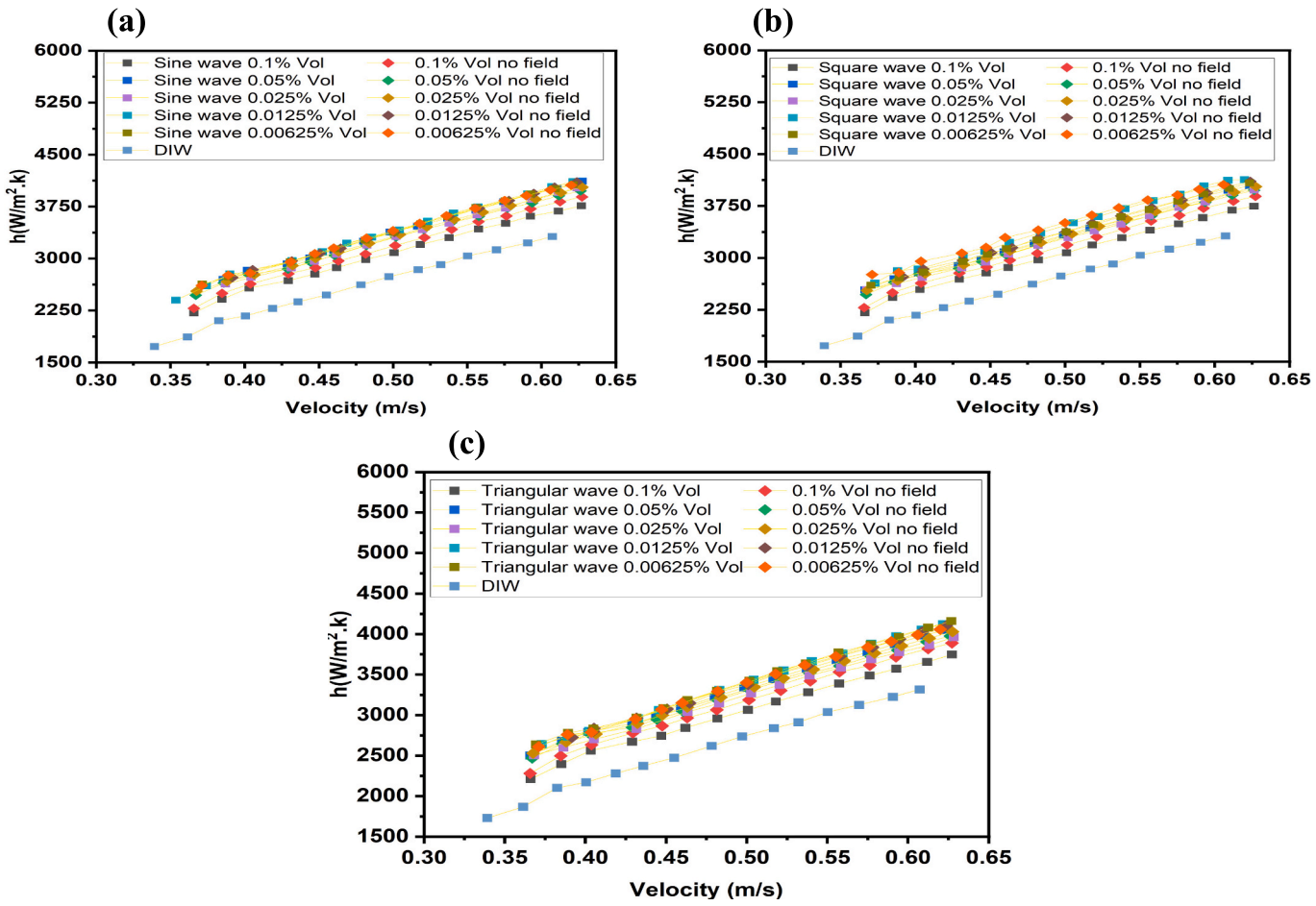

Fig. 20. Comparative analysis of heat transfer coefficients, magnetic hybrid nanofluids vs. deionized water across varying velocities and concentrations with magnetic waves and in the absence of magnetic fields Case IV (a) Sine waves (b) Square waves and (c) Triangular waves

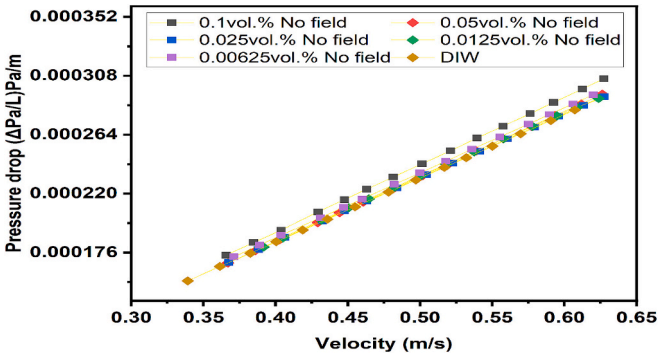

Fig. 21. Comparison of pressure drop between deionized water and magnetic hybrid nanofluids with no magnetic field at different concentrations across varied velocities Case I

wt% were examined. Among these concentrations, the TPF was noticed to be the highest at a concentration of 0.0125 %. This concentration showed promising potential and warranted further investigation into optimizing magnetic field positioning and the impact of various waveforms on fluid performance to draw valid conclusions for practical applications. Figs. 26**a, b**, and **c** compared different waveforms for **Case II**, **Case III**, and **Case IV**, respectively. The outcomes indicated that for **Case II** waveform, sine waves outperformed square waves and triangular waves along the flow velocity. Conversely, for **Case III,** triangular waves performed better than sine and square waves. Finally, in **Case IV**, square waves demonstrated superior performance along the flow velocity. These findings show the impact of MF placement and waveform on fluid thermal performance factors. Optimizing the best thermal performance for practical application is crucial and depends on the specific requirements of the heat transfer application. This analysis suggested the importance of considering magnetic field positioning and waveform selection in enhancing heat transfer efficiency in magnetic hybrid nanofluids for various practical applications.

The comparison of thermal performance factors for different magnetic hybrid nanofluid cases using sine waveforms at 0.0125 % volume fraction (Fig. 27a) reveals that Case II exhibits the best thermal performance among the cases tested. Across various velocities, **Case II** consistently demonstrates higher thermal performance factors compared to **Cases III** and **IV**. For instance, at a velocity of 0.623 m/s, the thermal performance factor for Case **II** ranges from approximately 1.189 to 1.231, while for **Case III** and **Case IV**, the values range from approximately 1.187 to 1.190 and 1.161 to 1.203, respectively. Several factors likely contribute to the superior performance of **Case II** with sine waves. Firstly, Case **II** may have optimized parameters or conditions that enhance convective heat transfer efficiency. Additionally, the smoother oscillations of sine waveforms may promote better fluid mixing and heat transfer compared to other waveforms like square or triangular waves. Moreover, the arrangement or positioning of the magnetic field in **Case II** might be more conducive to enhancing heat transfer within the nanofluid, potentially leading to improved thermal performance factors. Furthermore, the interaction between the magnetic field and nanoparticles in **Case II** under sine wave conditions could result in more favorable nanoparticle dispersion and alignment, further enhancing

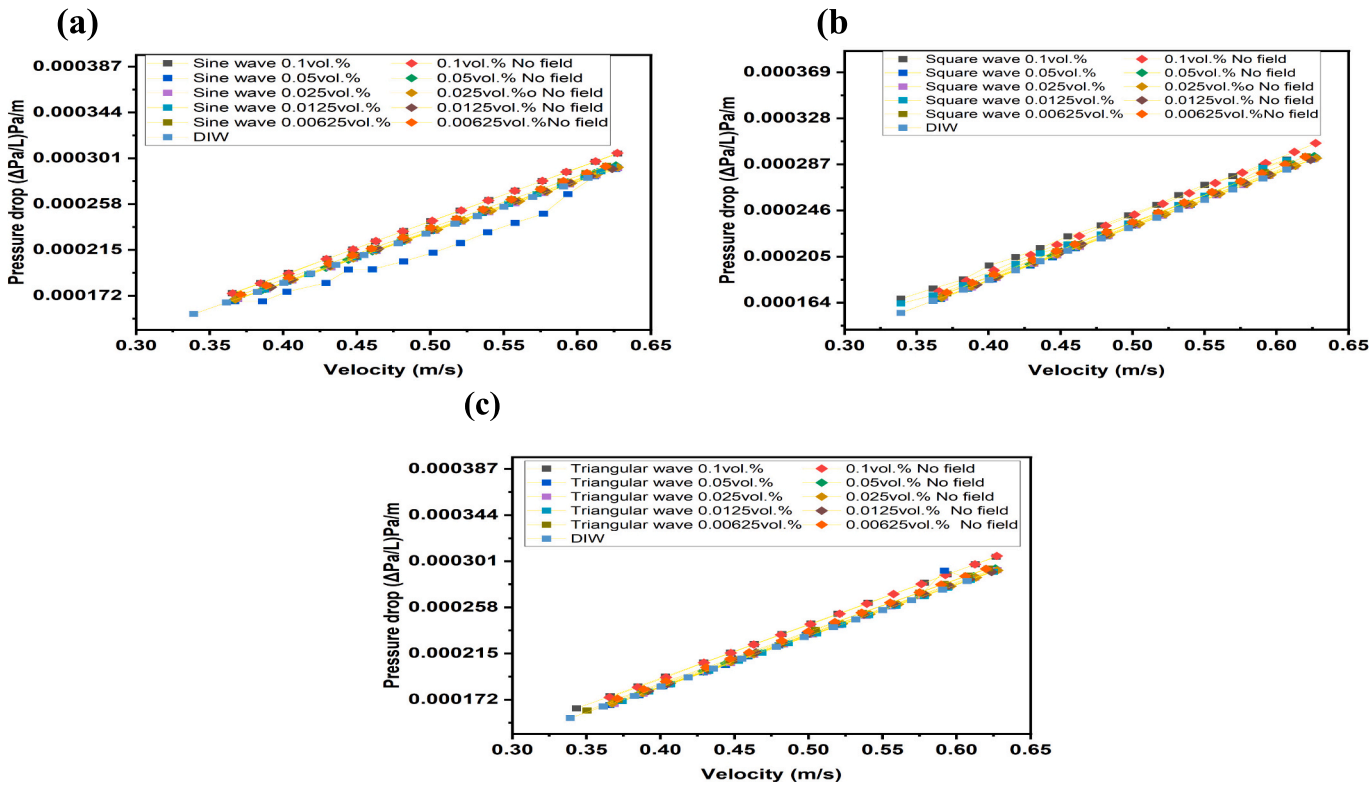

Fig. 22. Comparison of pressure drop between deionized water and magnetic hybrid nanofluids with no magnetic field at different concentrations across varied velocities Case II. (a) Sine waves (b) Square and (c) Triangular

convective heat transfer. Overall, compared to Cases III and IV, the combination of optimized parameters, waveform characteristics, and magnetic field positioning likely contributes to the superior thermal performance observed in Case II with sine waves.

In the comparison using square waveforms at 0.0125 % volume fraction (Fig. 27b), it is apparent that **Case IV** exhibits the best thermal performance factor among the cases. Analysing the velocities and corresponding thermal performance factor values reveals that **Case IV** with square waves generally demonstrates higher values compared to **Cases II** and **III**. This superiority in thermal performance can be attributed to the specific characteristics of the square wave magnetic field, which may induce optimal fluid flow patterns and enhance convective heat transfer within the nanofluid. Additionally, the interaction between the square wave magnetic field and the Fe_3O_4/TiO_2nanoparticles may lead to improved dispersion and alignment of nanoparticles, resulting in enhanced thermal conductivity and heat transfer efficiency. In summary, the unique characteristics of the square wave magnetic field likely contribute to the observed superior thermal performance in **Case IV** compared to **Cases II** and **III**.

Lastly, the comparison using triangular waveforms at 0.0125 % volume fraction **(**Fig. 27**c)** demonstrates that **Case II** exhibits the best thermal performance factor among the cases. Across various velocities, **Case II** consistently shows higher thermal performance factors compared to **Cases III** and **IV**. The superior thermal performance in Case **II** with triangular waves can be attributed to the specific characteristics of the triangular wave magnetic field, which may induce optimal fluid flow patterns and enhance convective heat transfer within the nanofluid. Additionally, the interaction between the triangular wave magnetic field and the Fe_3O_4/TiO_2nanoparticles may lead to improved dispersion and alignment of nanoparticles, resulting in enhanced thermal conductivity and heat transfer efficiency. Overall, the unique characteristics of the triangular wave magnetic field likely contribute to the observed superior thermal performance in **Case II** compared to **Cases III** and **IV.**

4.6. *Thermal entropy generation analysis of MHNFS nanofluids and influence of concentration and velocity*

The total entropy generation rate ($\dot{E}_{gen}$) in a cylindrical tube of length L encompasses both the thermal entropy generation rate ($E_{gen.Th}$) and the frictional entropy generation rate ($E_{gen.fl}$). This combined entropy generation rate is determined by the summation of these two components, as described in the following equations [53].

$$\dot{E}_{gen} = E_{gen.Th} + E_{gen.fl} \tag{23}$$

$$E_{gen.Th} = \frac{\pi d^2 L q^{-2}}{K_{nf} Nu T_{av}} \tag{24}$$

$$E_{gen.fl} = \frac{32\dot{m}^2 fl}{\rho_{nf}^2 \pi^2 d^5 T_{av}} \tag{25}$$

$$T_{avg} = \frac{(T_{in} - T_{out})}{In\left(\frac{T_{in}}{T_{out}}\right)} \tag{26}$$

The analysis presented in **Figs. 28a** demonstrates the impact of nanoparticle concentration on entropy generation in magnetic hybrid nanofluids (MHNFs) is notable. Decreasing nanoparticle concentration corresponds to a reduction in $E_{gen.Th}$. Furthermore, both total and $E_{gen.Th}$ diminish with increasing velocity. For instance, at a velocity of 0.431 m/s and a nanoparticle concentration of 0.00125 % vol, the $E_{gen.Th}$ is

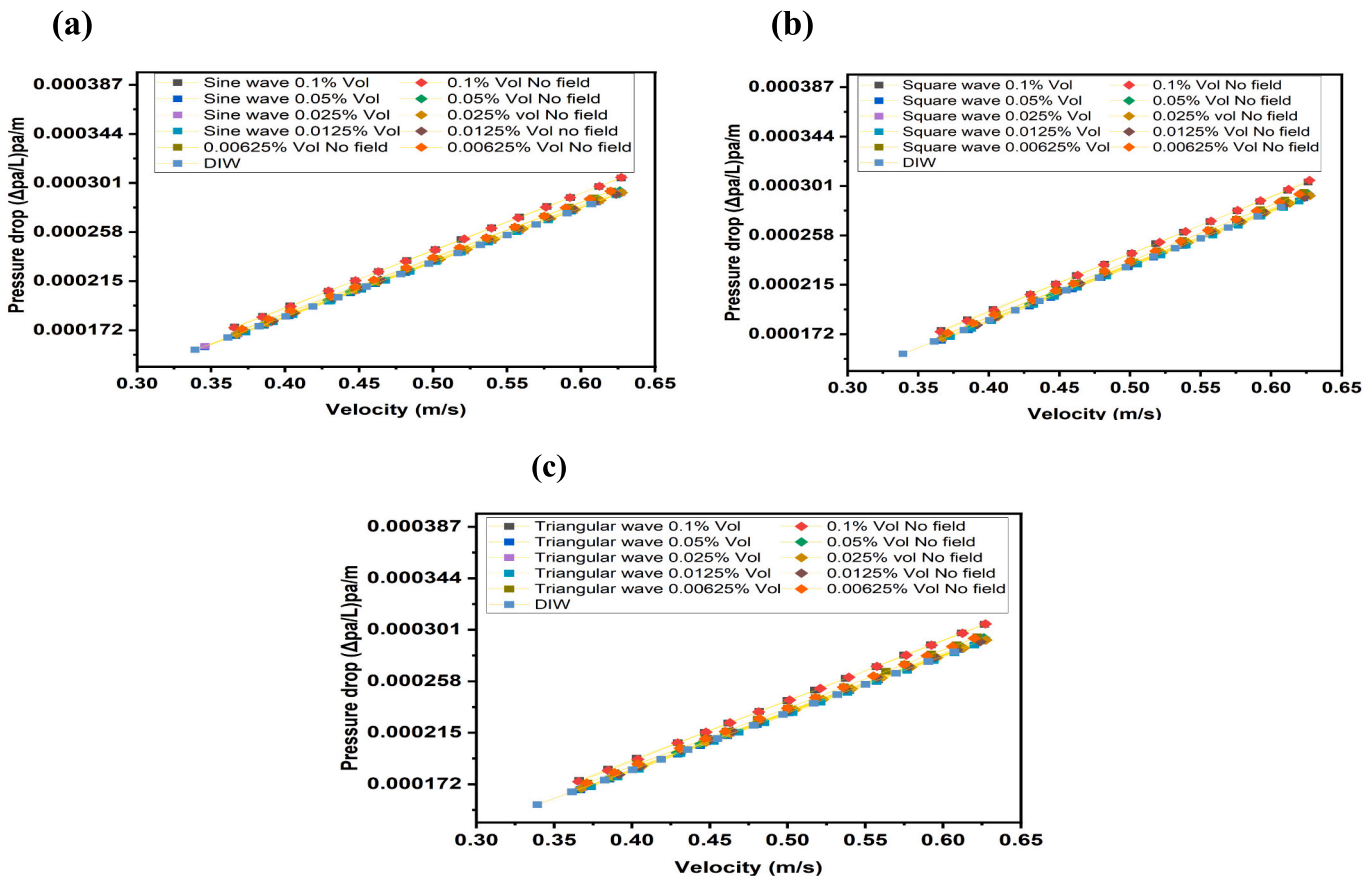

Fig. 23. Comparison of pressure drop between deionized water and magnetic hybrid nanofluids with no magnetic field at different concentrations across varied velocities case III. (a) sine (b) square and (c) triangular.

determined to be 27.666. Interestingly, at this velocity, the $E_{gen.Th}$ is lower compared to 0.05 % vol and 0.025 % vol, which exhibit $E_{gen.Th}$ of 28.3 at a velocity of 0.429 m/s and 27.82 at a velocity of 0.432 m/s, respectively.

The analysis suggests that lower velocities generally lead to higher $E_{gen.Th}$ rates across all concentrations. This phenomenon can be attributed to reduced CHT rates and slower fluid motion at lower velocities, resulting in higher temperature gradients and, as a result, higher entropy generation within the system. Conversely, higher velocities facilitate more efficient heat transfer by promoting fluid mixing and reducing temperature gradients, leading to lower entropy generation rates. Therefore, optimizing velocity conditions is crucial to minimizing thermal losses and improving the efficiency of heat transfer processes involving MHNFs. By controlling velocity parameters, it is possible to enhance heat transfer efficiency and reduce $E_{gen.Th}$ in MHNF systems, ultimately improving their overall performance.

Fig. 28 **(b)** demonstrates a rise in $E_{gen.fl}$ with increasing MHNFs nanofluid concentration. Conversely, it is evident that as the concentration of MHNFs decreases, $E_{gen.fl}$ also decreases accordingly. For instance, at a velocity of 0.623 m/s, the $E_{gen.fl}$ decreases from approximately 1.69532E-09 for a concentration of 0.1 % to 5.51537E-10 for a concentration of 0.00625 %. This trend suggests that lower concentrations of MHNFs result in improved hydrodynamic efficiency, with lower frictional losses within the heat transfer system. Furthermore, the analysis reveals that higher velocities generally correspond to higher $E_{gen.fl}$ rates across all concentrations, but values were extremely very low which can be neglected. For instance, at a concentration of 0.0125 %, the $E_{gen.fl}$ increases from approximately 1.55641E-09 at a velocity of 0.623 m/s to 7.10846E-10 at a velocity of 0.391609769 m/s. These findings show the importance of optimizing flow conditions to minimize frictional losses and enhance the efficiency of heat transfer processes involving MHNFs. Furthermore, the results suggest that lower MHNFs nanofluids concentrations can be effectively utilized as working fluids in thermal energy systems, as they show negligible effects from rises in fluid viscosity and pressure drop, these observations suggest the possibility of improving forced CHT while concurrently reducing E_{gen} by lowering the concentration of MHNFs nanoparticles.

4.7. Entropy generation in heat transfer systems of magnetic hybrid nanofluids: effects of magnetic field positioning and waveforms

Fig. 29 **(a), c**, and **e** display **Case II**, **Case III**, and **Case IV**, respectively, representing the positioning of the magnetic field along the test section. These figures indicate that the $E_{gen.Th}$ rate of the magnetic nanofluid diminishes with the application of a magnetic field, and furthermore, thermal entropy generation decreases with velocity. In Fig. 27(a), it is evident that magnetic forces can enhance heat transfer, with the most significant enhancement observed in Case II with square waves at a fluid velocity of 0.375 m/s. Moreover, it is observed that the total entropy generation rate is decreased by up to 4.28 % compared to the absence of a magnetic field, with reductions of 2.2 % for sine waves

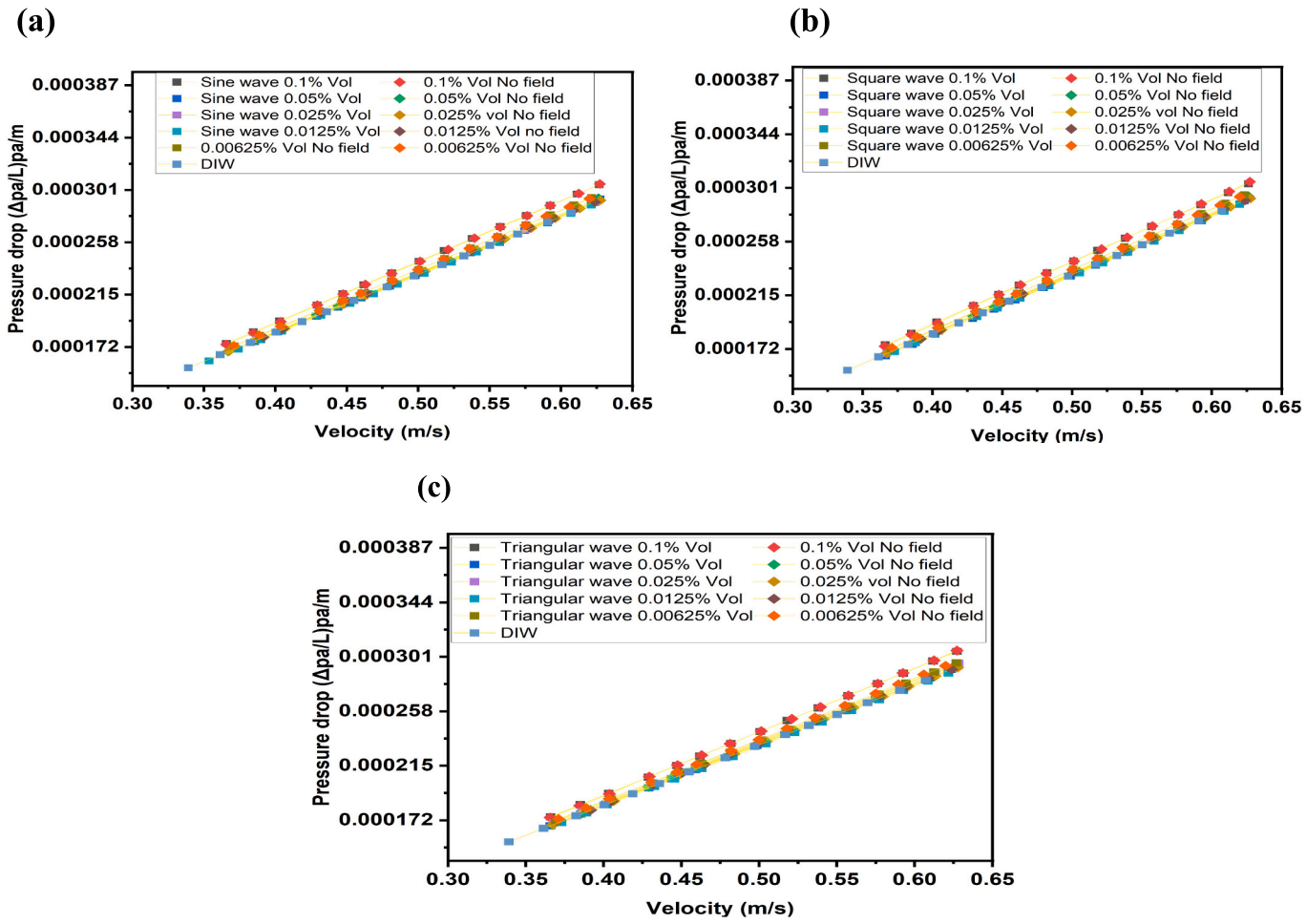

Fig. 24. Comparison of pressure drop between deionized water and magnetic hybrid nanofluids with magnetic field at different concentrations across varied velocities Case IV

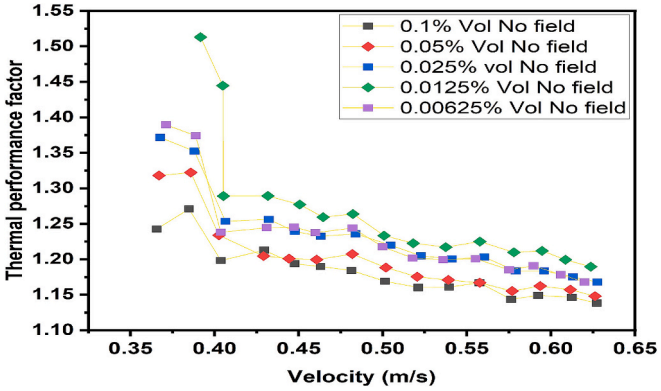

Fig. 25. Thermal performance factor against velocity for different volume concentrations of MHNFs

and 2.73 % for triangular waves, respectively. However, **Case III** shows that the applied magnetic forces lead to less enhancement of heat transfer compared to other cases, with a total entropy generation rate reduction of up to 1.79 % at a fluid velocity of 0.375 m/s compared to without a magnetic field, with reductions of 0.1 % for square waves and 0.3 % for sine waves. This difference could be attributed to the magnetic field positioning. Meanwhile, **Case IV** shows that magnetic forces can enhance heat transfer, with the best performance observed with triangular waves, resulting in a reduction of up to 1.65 % at a fluid velocity of 0.375 m/s, followed by square waves with 1.5 % and sine waves with 0.9 % reduction. Several factors contribute to the improved heat transfer observed after the application of different magnetic waveforms. Specifically, the augmentation in thermal conductivity and viscosity resulting from the accumulation of magnetic particles near the inner wall surface induces a modification in the thickness of the thermal boundary layer. In accordance with fluid dynamic principles, the enhancement of heat transfer in magnetic hybrid nanofluids (MHNFs) can be achieved by examining the relationship between thermal conductivity and the thickness of the boundary layer [14]. Moreover, the migration of magnetic particles towards the tube wall due to the influence of the magnetic field can also contribute to this phenomenon., thereby further amplifying heat transfer properties [25].

Fig. 29 **(b), d, f**, depict **Case II**, **Case III**, and **Case IV**, respectively, representing the magnetic field position along the test section. These figures show that the frictional entropy generation rate increases with velocity, although the enhancement of frictional entropy generation is negligible.

Additionally, the findings indicate that lower concentrations of MHNFs can serve as efficient working fluids in thermal energy systems, as they demonstrate limited sensitivity to rises in fluid viscosity and pressure drop. These results suggest the possibility of improving forced CHT while concurrently boosting the reduction in total entropy generation by lowering the concentration of MHNFs nanoparticles.

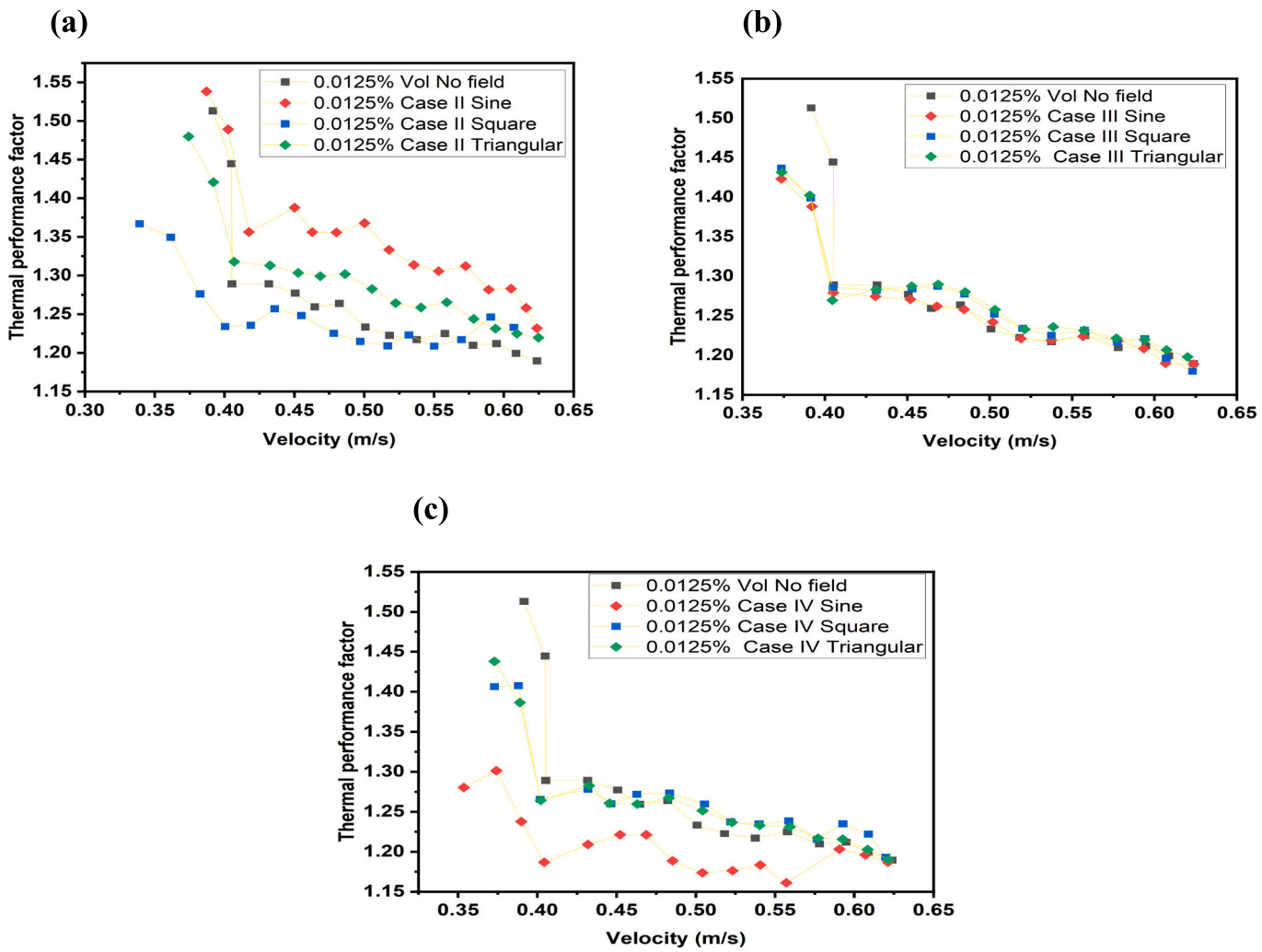

Fig. 26. Comparison of thermal performance factors with different magnetic field positions and waveforms in magnetic hybrid nanofluids. (a) Comparing Case II waveform (b) Comparing Case III waveform and (c) Comparing Case IV waveform

5. Conclusion

This study explored heat transfer, entropy generation, and thermal performance factor analysis of Fe_3O_4/TiO_2 magnetic hybrid nanofluids, focusing on the influence of magnetic waveform positioning in a turbulent flow regime.

In conclusion, the findings emphasize the substantial role of magnetic field waves in enhancing heat transfer in Fe_3O_4/TiO_2 nanofluids. Experimental tests across different waveform types and volume fractions consistently demonstrated improvements in heat transfer efficiency, especially at lower volume fractions. Among the waveform types, square waves proved the most effective, achieving higher enhancement percentages in various cases. The precise positioning of thermocouples and optimization of magnetic field parameters, particularly in the fully developed thermal region, were essential for accurate heat transfer coefficient measurements.

- The study underscores the importance of optimizing magnetic field parameters such as waveform selection and positioning to improve convective heat transfer efficiency in Fe_3O_4/TiO_2magnetic hybrid nanofluids. Results suggest that different waveform configurations (e.g., sine, square, and triangular) have varying effects on thermal performance, with sine waves (**Case II**) yielding the most favorable outcomes.
- Regarding nanofluid concentration, lower concentrations of Fe_3O_4/TiO_2 nanoparticles exhibited significant potential for efficient use in thermal energy systems. These lower concentrations had minimal impact on fluid viscosity and pressure drop while enhancing convective heat transfer efficiency, indicating practical applications for such fluids in diverse thermal systems.
- The application of a magnetic field also contributed to reduced thermal entropy generation rates, especially when paired with optimized magnetic field settings. This reduction, combined with improved convective heat transfer efficiency, indicates enhanced thermal performance and energy efficiency in systems utilizing Fe_3O_4/TiO_2 magnetic hybrid nanofluids.

This research emphasizes the importance of optimizing magnetic field parameters, such as waveform selection and positioning, to maximize heat transfer efficiency. It also suggests that lower concentrations of Fe_3O_4/TiO_2 nanoparticles could be utilized efficiently in thermal systems, offering minimal impact on fluid viscosity and pressure drop while enhancing heat transfer.

Future research directions include further optimization of magnetic field parameters and exploring additional waveform configurations to

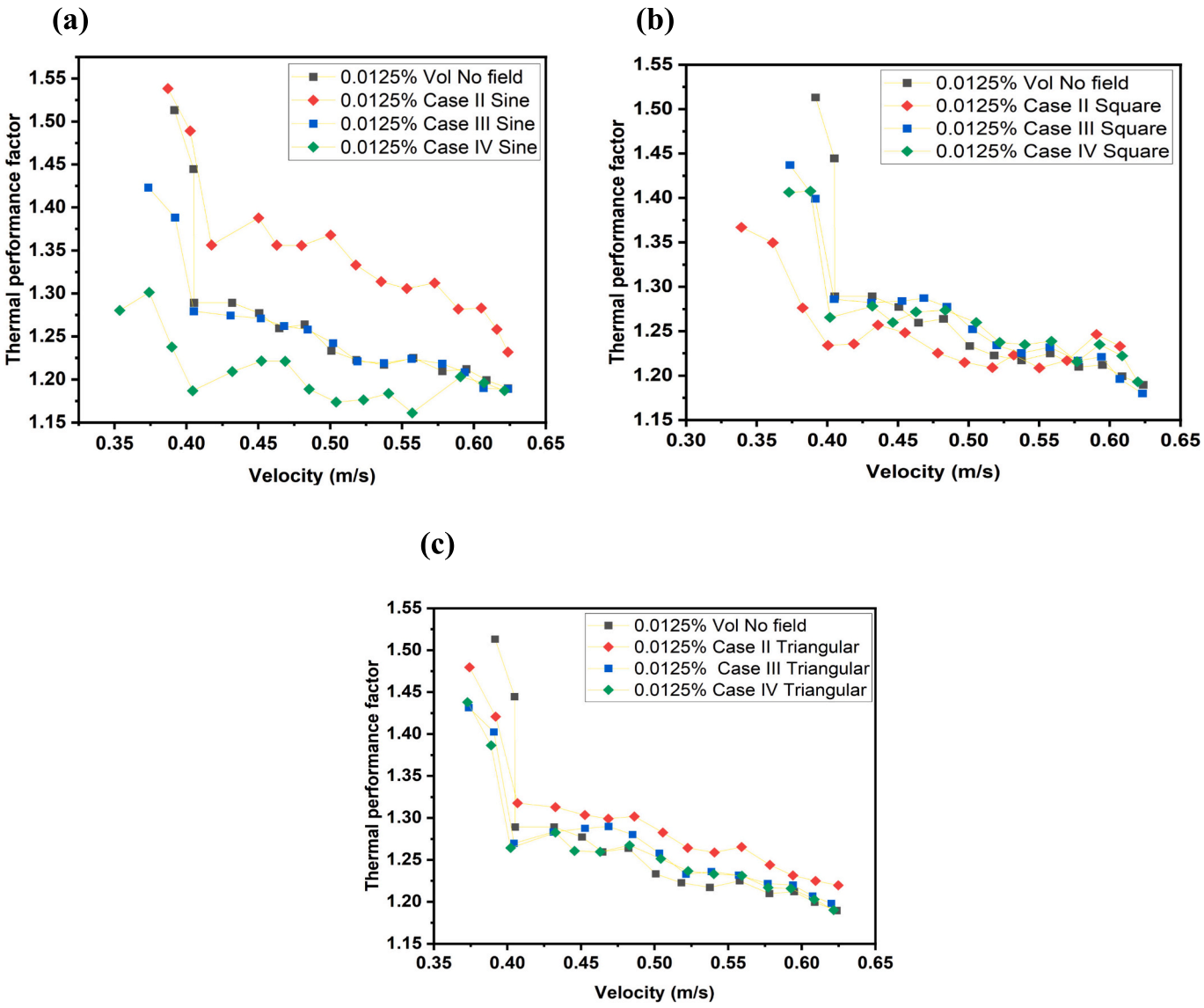

Fig. 27. Comparison of thermal performance factors with different waveforms and magnetic field cases at 0.0125 % volume fraction. (a) comparing all cases sine waveform (b) comparing all cases square waveform and (c) Comparing all cases of triangular waveform.

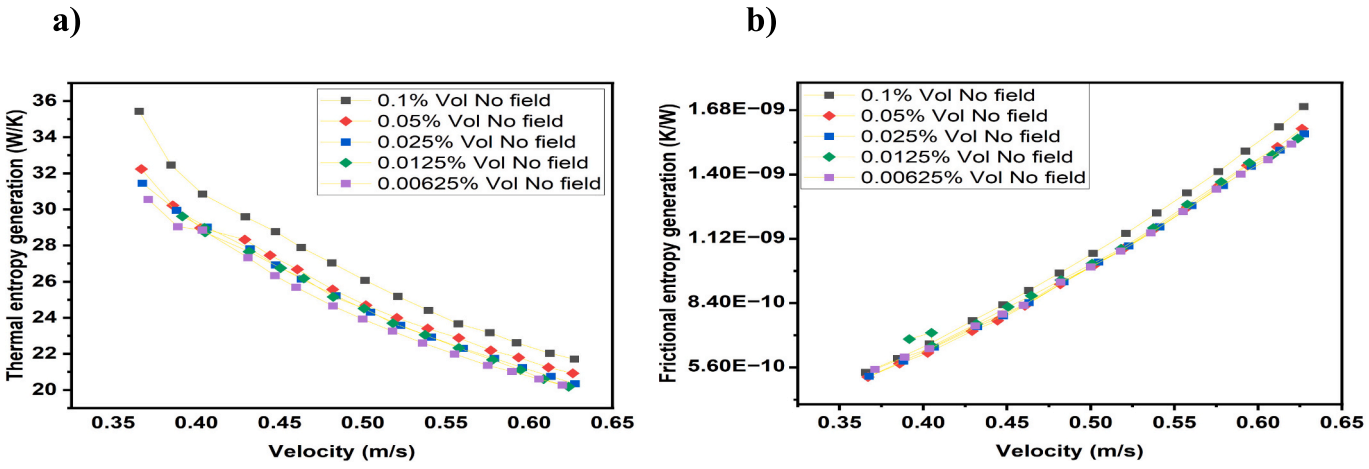

Fig. 28. Entropy generation rate analysis of MHNFS nanofluids with no external magnetic field with the influence of velocity and concentration on a) thermal entropy generation and b) frictional entropy generation components.

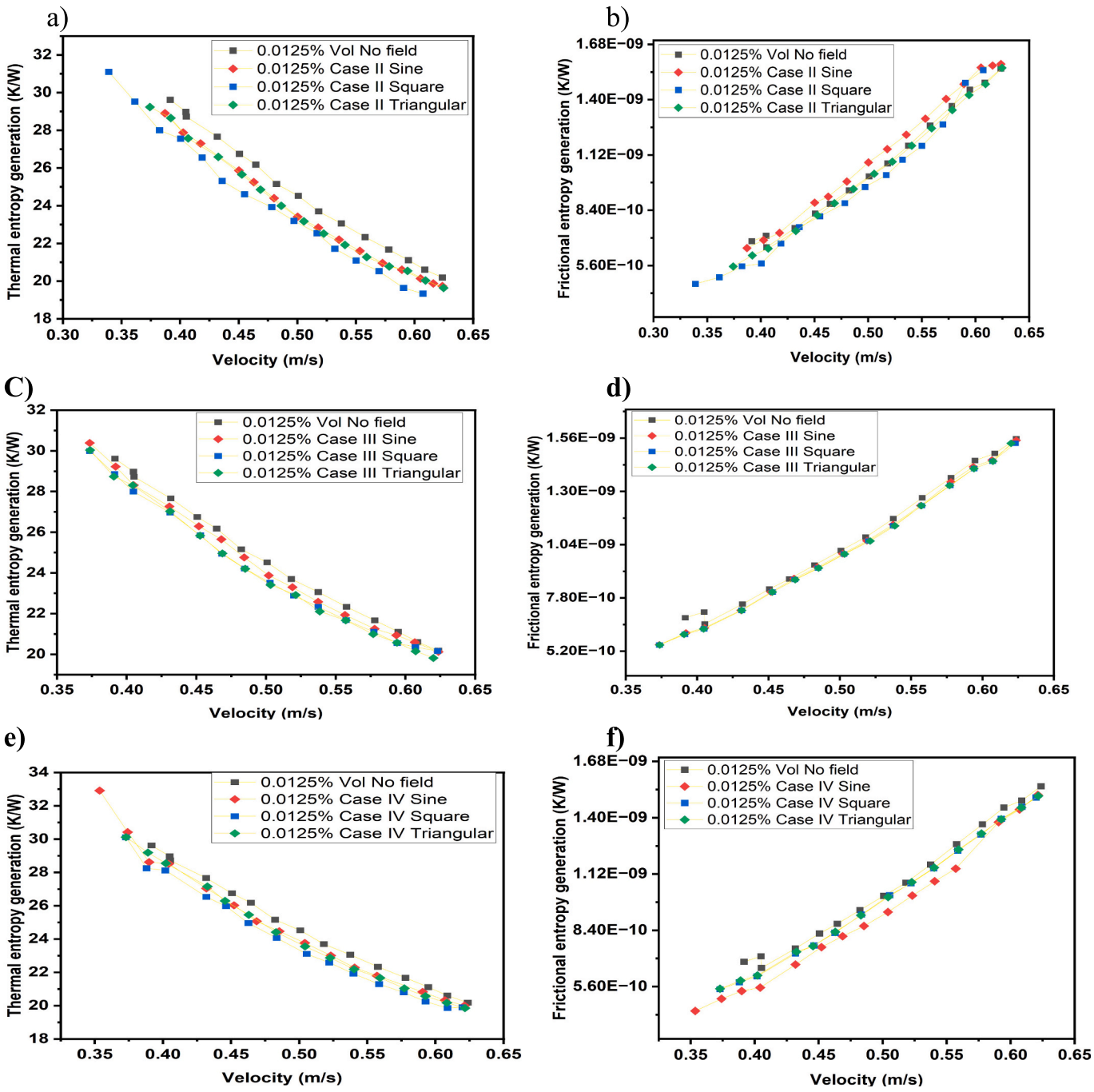

Fig. 29. Entropy generation rate analysis of MHNFS nanofluids with no external magnetic field with influence of velocity and concentration on (a) case II (c) case III and (e) case IV on thermal entropy generation and (b) case II (d) case III and (f) case IV on frictional entropy generation components.

improve convective heat transfer and minimize entropy generation. Additionally, future work should focus on optimizing nanoparticle composition and size, assessing long-term stability, and numerical modeling and simulation could provide deeper insights, while research on flow regimes beyond turbulence could offer a broader understanding of nanofluid performance. Scaling and real-world industrial integration, alongside environmental and safety considerations, are also vital areas for further exploration to ensure the practical and sustainable application of Fe_3O_4/TiO_2 magnetic hybrid nanofluids in thermal energy systems.

CRediT authorship contribution statement

Victor O. Adogbeji: Writing – original draft, Visualization, Validation, Resources, Investigation, Formal analysis, Data curation, Conceptualization. **Kuvendran Govinder:** Writing – original draft, Validation, Investigation, Formal analysis, Data curation. **Mohsen Sharifpur:** Writing – review & editing, Validation, Supervision, Resources, Project administration, Methodology, Funding acquisition, Conceptualization. **Josua P. Meyer:** Writing – review & editing, Validation, Supervision, Resources, Methodology, Funding acquisition.

Declaration of competing interest

The authors declare that there are no financial or personal conflicts of interest that could be perceived as influencing the outcomes of this research.

Data availability

Data supporting this study is available upon request. Further investigation is recommended to deepen understanding and improve optimization for various practical uses.

References

[1] S.U.S. Choi, J.A. Eastman, Enhancing thermal conductivity of fluids with. ASME Int Mech Eng Congr Expo.1995 66, 1995, pp. 99–105, https://doi.org/10.1115/1.1532008, p. 1995.

[2] A.S. John, B. Mahanthesh, I.V. Shevchuk, Study of nanofluid flow and heat transfer in a stationary cone-disk system, Therm. Sci. Eng. Prog. 46 (June) (2023) 102173, https://doi.org/10.1016/j.tsep.2023.102173.

[3] V.O. Adogbeji, E.O. Atofarati, M. Sharifpur, J.P. Meyer, Experimental investigation and machine learning modeling of the effects of hybridization mixing ratio, nanoparticle type, and temperature on the thermophysical properties of - Fe 3 O 4 / TiO 2, – Fe 3 O 4 / MgO, and - Fe 3 O 4 / ZnO - DI water hybrid ferrofluids, J. Therm. Anal. Calorim. (2025), https://doi.org/10.1007/s10973-025-14399-y.

[4] P. Ganesh Kumar, V.S. Vigneswaran, V. Sivalingam, R. Velraj, S.C. Kim, V. Ramkumar, Enhancing heat transfer performance of automotive radiator with H2O / activated carbon nanofluids, J. Mol. Liq. 371 (2023) 121153, https://doi.org/10.1016/j.molliq.2022.121153.

[5] I.U. Ibrahim, M. Sharifpur, J.P. Meyer, S.M.S. Murshed, Experimental investigations of effects of nanoparticle size on force convective heat transfer characteristics of Al2O3 - MWCNT hybrid nanofluids in transitional flow regime, Int. J. Heat Mass Transf. 228 (June 2023) (2024) 125597, https://doi.org/10.1016/j.ijheatmasstransfer.2024.125597.

[6] V. Baldin, L.R.R. da Silva, A.R. Machado, C.F. Houck, State of the Art of Biodegradable Nanofluids Application in Machining Processes vol. 10, no. 5, Korean Society for Precision Engineering, 2023, https://doi.org/10.1007/s40684-022-00486-0.

[7] V.O. Adogbeji, E.O. Atofarati, M. Sharifpur, J.P. Meyer, Magnetohydrodynamics of nanofluid internal forced convection : a review and outlook for practical applications, Results Phys 68 (October 2024) (2025) 108082, https://doi.org/10.1016/j.rinp.2024.108082.

[8] M. Gürdal, H.K. Pazarlıoğlu, M. Tekir, F.M. Altunay, K. Arslan, E. Gedik, Implementation of hybrid nanofluid flowing in dimpled tube subjected to magnetic field, Int. Commun. Heat Mass Transf. 134 (2022), https://doi.org/10.1016/j.icheatmasstransfer.2022.106032.

[9] U. Nithiyanantham, et al., Effect of silica nanoparticle size on the stability and thermophysical properties of molten salts based nanofluids for thermal energy storage applications at concentrated solar power plants, J Energy Storage 51 (March) (2022), https://doi.org/10.1016/j.est.2022.104276.

[10] A. Lee, C. Veerakumar, H. Cho, Effect of magnetic field on the forced convective heat transfer of water–ethylene glycol-based fe3 o4 and fe3 o4 –mwcnt nanofluids, Appl. Sci. 11 (10) (May 2021), https://doi.org/10.3390/app11104683.

[11] S.V. Mousavi, M. Sheikholeslami, M. Gorji Bandpy, M. Barzegar Gerdroodbary, The influence of magnetic field on heat transfer of magnetic nanofluid in a sinusoidal double pipe heat exchanger, Chem. Eng. Res. Des. 113 (2016) 112–124, https://doi.org/10.1016/j.cherd.2016.07.009.

[12] N. Hatami, A. Kazemnejad Banari, A. Malekzadeh, A.R. Pouranfard, The effect of magnetic field on nanofluids heat transfer through a uniformly heated horizontal tube, Phys. Lett. Sect. A Gen. At. Solid State Phys. 381 (5) (2017) 510–515, https://doi.org/10.1016/j.physleta.2016.12.017.

[13] L. Sha, Y. Ju, H. Zhang, The influence of the magnetic field on the convective heat transfer characteristics of Fe3O4/water nanofluids, Appl. Therm. Eng. 126 (2017) 108–116, https://doi.org/10.1016/j.applthermaleng.2017.07.150.

[14] M. Yarahmadi, H. Moazami Goudarzi, M.B. Shafii, Experimental investigation into laminar forced convective heat transfer of ferrofluids under constant and oscillating magnetic field with different magnetic field arrangements and oscillation modes, Exp. Thermal Fluid Sci. 68 (2015) 601–611, https://doi.org/10.1016/j.expthermflusci.2015.07.002.

[15] A. Abadeh, M. Sardarabadi, M. Abedi, M. Pourramezan, M. Passandideh-Fard, M. J. Maghrebi, Experimental characterization of magnetic field effects on heat transfer coefficient and pressure drop for a ferrofluid flow in a circular tube, J. Mol. Liq. 299 (2020), https://doi.org/10.1016/j.molliq.2019.112206.

[16] B. Sun, Y. Guo, D. Yang, H. Li, The effect of constant magnetic field on convective heat transfer of Fe3O4/water magnetic nanofluid in horizontal circular tubes, Appl. Therm. Eng. 171 (December 2019) (2020) 114920, https://doi.org/10.1016/j.applthermaleng.2020.114920.

[17] M. Goharkhah, A. Salarian, M. Ashjaee, M. Shahabadi, Convective heat transfer characteristics of magnetite nanofluid under the influence of constant and alternating magnetic field, Powder Technol. 274 (2015) 258–267, https://doi.org/10.1016/j.powtec.2015.01.031.

[18] Y. Xuan, Q. Li, M. Ye, Investigations of convective heat transfer in ferrofluid microflows using lattice-Boltzmann approach, Int J Therm Sci 46 (2) (2007) 105–111, https://doi.org/10.1016/j.ijthermalsci.2006.04.002.

[19] M. Motozawa, J. Chang, T. Sawada, Y. Kawaguchi, Effect of magnetic field on heat transfer in rectangular duct flow of a magnetic fluid, Phys. Procedia 9 (2) (2010) 190–193, https://doi.org/10.1016/j.phpro.2010.11.043.

[20] M. Şeşen, et al., Heat transfer enhancement with actuation of magnetic nanoparticles suspended in a base fluid, J. Appl. Phys. 112 (6) (2012), https://doi.org/10.1063/1.4752729.

[21] Q. Li, Y. Xuan, Experimental investigation on heat transfer characteristics of magnetic fluid flow around a fine wire under the influence of an external magnetic field, Exp. Thermal Fluid Sci. 33 (4) (2009) 591–596, https://doi.org/10.1016/j.expthermflusci.2008.12.003.

[22] S. Mei, C. Qi, T. Luo, X. Zhai, Y. Yan, Effects of magnetic field on thermo-hydraulic performance of Fe3O4-water nanofluids in a corrugated tube, Int. J. Heat Mass Transf. 128 (2019) 24–45, https://doi.org/10.1016/j.ijheatmasstransfer.2018.08.071.

[23] R. Azizian, E. Doroodchi, T. McKrell, J. Buongiorno, L.W. Hu, B. Moghtaderi, Effect of magnetic field on laminar convective heat transfer of magnetite nanofluids, Int. J. Heat Mass Transf. 68 (2014) 94–109, https://doi.org/10.1016/j.ijheatmasstransfer.2013.09.011.

[24] J. Wang, G. Li, H. Zhu, J. Luo, B. Sundén, Experimental investigation on convective heat transfer of ferrofluids inside a pipe under various magnet orientations, Int. J. Heat Mass Transf. 132 (2019) 407–419, https://doi.org/10.1016/j.ijheatmasstransfer.2018.12.023.

[25] M. Mehrali, et al., Heat transfer and entropy generation analysis of hybrid graphene/Fe3O4 ferro-nanofluid flow under the influence of a magnetic field, Powder Technol. 308 (2017) 149–157, https://doi.org/10.1016/j.powtec.2016.12.024.

[26] A. Shahsavar, M. Saghafian, M.R. Salimpour, M.B. Shafii, Experimental investigation on laminar forced convective heat transfer of ferrofluid loaded with carbon nanotubes under constant and alternating magnetic fields, Exp. Thermal Fluid Sci. 76 (2016) 1–11, https://doi.org/10.1016/j.expthermflusci.2016.03.010.

[27] M. Tekir, E. Taskesen, E. Gedik, K. Arslan, B. Aksu, Effect of constant magnetic field on Fe3O4-Cu/water hybrid nanofluid flow in a circular pipe, Heat Mass Transf. und Stoffuebertragung 58 (5) (2022) 707–717, https://doi.org/10.1007/s00231-021-03125-7.

[28] L. Shi, Y. Hu, Y. He, Magnetocontrollable convective heat transfer of nanofluid through a straight tube, Appl. Therm. Eng. 162 (March) (2019) 114220, https://doi.org/10.1016/j.applthermaleng.2019.114220.

[29] H. Talebi, M.H. Kalantar, V. Nazari, M.R. Kargarsharifabad, Experimental investigation of the forced convective heat transfer of hybrid cu / Fe3O4 nanofluids, J. Solid Fluid Mech. 8 (4) (2019) 229–238, https://doi.org/10.22044/jsfm.2019.7350.2687.

[30] J. Alsarraf, R. Rahmani, A. Shahsavar, M. Afrand, S. Wongwises, M.D. Tran, Effect of magnetic field on laminar forced convective heat transfer of MWCNT–Fe3O4/water hybrid nanofluid in a heated tube, J. Therm. Anal. Calorim. 137 (5) (2019) 1809–1825, https://doi.org/10.1007/s10973-019-08078-y.

[31] X. Zhang, Y. Zhang, Experimental study on enhanced heat transfer and flow performance of magnetic nanofluids under alternating magnetic field, Int J Therm Sci 164 (January) (2021) 106897, https://doi.org/10.1016/j.ijthermalsci.2021.106897.

[32] S.O. Giwa, M. Sharifpur, J.P. Meyer, Experimental study of thermo-convection performance of hybrid nanofluids of Al2O3-MWCNT/water in a differentially heated square cavity, Int. J. Heat Mass Transf. 148 (2020), https://doi.org/10.1016/j.ijheatmasstransfer.2019.119072.

[33] V.O. Adogbeji, M. Sharifpur, J.P. Meyer, Experimental investigation into heat transfer and flow characteristics of magnetic hybrid nanofluid (Fe 3 O 4 / TiO 2) in turbulent region, Appl. Therm. Eng. 258 (PA) (2025) 124630, https://doi.org/10.1016/j.applthermaleng.2024.124630.

[34] V.O. Adogbeji, M. Sharifpur, J.P. Meyer, Experimental investigation of heat transfer enhancement, thermal efficiency, and pressure drop in forced convection of magnetic hybrid nanofluid (Fe_3O_4 / TiO_2) under varied magnetic field strengths and waveforms, Case Stud. Therm. Eng. 63 (June) (2024) 105313, https://doi.org/10.1016/j.csite.2024.105313.

[35] D.P. Kulkarni, P.K. Namburu, H. Ed Bargar, D.K. Das, Convective heat transfer and fluid dynamic characteristics of SiO 2 - ethylene glycol/water nanofluid, Heat Transf. Eng. 29 (12) (2008) 1027–1035, https://doi.org/10.1080/01457630802243055.

[36] B.C. Pak, Y.I. Cho, Hydrodynamic and heat transfer study of dispersed fluids with submicron metallic oxide particles, Exp. Heat Transf. 11 (2) (1998) 151–170, https://doi.org/10.1080/08916159808946559.

[37] A.J. Ghajar, L.M. Tam, Heat transfer measurements and correlations in the transition region for a circular tube with three different inlet configurations, Exp. Thermal Fluid Sci. 8 (1) (1994) 79–90, https://doi.org/10.1016/0894-1777(94)90075-2.

[38] E. Sadeghinezhad, et al., Experimental study on heat transfer augmentation of graphene based ferrofluids in presence of magnetic field, Appl. Therm. Eng. 114 (2017) 415–427, https://doi.org/10.1016/j.applthermaleng.2016.11.199.

[39] J.A. Olivier, J.P. Meyer, Single-phase heat transfer and pressure drop of the cooling of water inside smooth tubes for transitional flow with different inlet geometries (rp-1280), HVAC R Res. 16 (4) (2010) 471–496, https://doi.org/10.1080/10789669.2010.10390916.

[40] V.O. Adogbeji, M. Sharifpur, J.P. Meyer, Experimental investigation of heat transfer, thermal efficiency, pressure drop, and flow characteristics of Fe 3 O 4

-MgO magnetic hybrid nanofluid in transitional flow regimes, Int J Therm Sci 209 (2025) 109515, https://doi.org/10.1016/j.ijthermalsci.2024.109515.
[41] P.F. Dunn, Measurement and Data Analysis for Engineering and Science Second Edition, Taylor and Francis / CRC Press, 2010, pp. 1–7, c 2010 ISBN : 9781439825686," no. August 2009.
[42] S. Osman, M. Sharifpur, J.P. Meyer, Experimental examination of transitional flow of dilute alumina - Water nanofluid, in: International Heat Transfer Conference vol. 2018-Augus, 2018, pp. 3095–3102, https://doi.org/10.1615/ihtc16.cov.023235.
[43] S.O. Giwa, M. Sharifpur, M.H. Ahmadi, S.M. Sohel Murshed, J.P. Meyer, Experimental investigation on stability, viscosity, and electrical conductivity of water-based hybrid nanofluid of mwcnt-fe2o3, Nanomaterials 11 (1) (2021) 1–19, https://doi.org/10.3390/nano11010136.
[44] S. Osman, M. Sharifpur, J.P. Meyer, Experimental investigation of convection heat transfer in the transition flow regime of aluminium oxide-water nanofluids in a rectangular channel, Int. J. Heat Mass Transf. 133 (2019) 895–902, https://doi.org/10.1016/j.ijheatmasstransfer.2018.12.169.
[45] A. Arifutzzaman, A.F. Ismail, I.I. Yaacob, M.Z. Alam, A.A. Khan, Stability investigation of water based exfoliated graphene nanofluids, IOP Conf. Ser. Mater. Sci. Eng. 488 (1) (2019), https://doi.org/10.1088/1757-899X/488/1/012002.
[46] S. Chakraborty, P.K. Panigrahi, Stability of nanofluid: A review, in: Applied Thermal Engineering vol. 174, Elsevier Ltd, Jun. 25, 2020, https://doi.org/10.1016/j.applthermaleng.2020.115259.
[47] M. Zadkhast, D. Toghraie, A. Karimipour, Developing a new correlation to estimate the thermal conductivity of MWCNT-CuO/water hybrid nanofluid via an experimental investigation, J. Therm. Anal. Calorim. 129 (2) (2017) 859–867, https://doi.org/10.1007/s10973-017-6213-8.
[48] A. Oraon, et al., Impact of magnetic field on the thermal properties of chemically synthesized Sm-Co nanoparticles based silicone oil nanofluid, J. Therm. Anal. Calorim. 147 (3) (2022) 1933–1943, https://doi.org/10.1007/s10973-021-10572-1.
[49] S. Suseel Jai Krishnan, M. Momin, C. Nwaokocha, M. Sharifpur, J.P. Meyer, An empirical study on the persuasive particle size effects over the multi-physical properties of monophase MWCNT-Al2O3 hybridized nanofluids, J. Mol. Liq. 361 (2022) 119668, https://doi.org/10.1016/j.molliq.2022.119668.
[50] M. Ashjaee, M. Goharkhah, L.A. Khadem, R. Ahmadi, Effect of magnetic field on the forced convection heat transfer and pressure drop of a magnetic nanofluid in a miniature heat sink, Heat Mass Transf. und Stoffuebertragung 51 (7) (2015) 953–964, https://doi.org/10.1007/s00231-014-1467-1.
[51] L.S. Sundar, M.K. Singh, A.C.M. Sousa, Enhanced heat transfer and friction factor of MWCNT-Fe3O4/water hybrid nanofluids, Int. Commun. Heat Mass Transf. 52 (Mar. 2014) 73–83, https://doi.org/10.1016/j.icheatmasstransfer.2014.01.012.
[52] S. Suresh, M. Chandrasekar, S. Chandra Sekhar, Experimental studies on heat transfer and friction factor characteristics of CuO/water nanofluid under turbulent flow in a helically dimpled tube, Exp. Thermal Fluid Sci. 35 (3) (2011) 542–549, https://doi.org/10.1016/j.expthermflusci.2010.12.008.
[53] G. Saha, M.C. Paul, Heat transfer and entropy generation of turbulent forced convection flow of nanofluids in a heated pipe, Int. Commun. Heat Mass Transf. 61 (2015) 26–36, https://doi.org/10.1016/j.icheatmasstransfer.2014.11.007.